Pliocene and Pleistocene stratigraphic evolution of the western Niger Delta intraslope basins: A record of glacio-eustatic sea-level and basin tectonic forcings

Kelvin Ikenna Chima, Christian Gorini, Marina Rabineau, Didier Granjeon, Damien Do Couto, Estelle Leroux, Nick Hoggmascall

Pliocene and Pleistocene stratigraphic evolution of the western Niger Delta intraslope basins: A record of glacio-eustatic sea-level and basin tectonic forcings

Kelvin Ikenna Chima[a,b]*, Christian Gorini[a], Marina Rabineau[c], Didier Granjeon[d], Damien Do Couto[a], Estelle Leroux[e], Nick Hoggmascall[f]

[a] Sorbonne Université-ISTeP UMR 7193, F7500, Paris (France)

[b] Alex Ekwueme Federal University, Ndufu-Alike Ikwo, Ebonyi State, Nigeria.

[c] CNRS, UMR 6538, LGO (CNRS/UBO/UBS), Plouzane (France)

[d] IFPEN, Rueil-Malmaison (France)

[e] IFREMER, ZI Pointe du Diable, Plouzane, France (France)

[f] Shell International (UK).

Abstract

Although climate proxy ($\delta^{18}O$) across the world ocean basins reveals that orbital forcing significantly controlled the Pliocene and the Pleistocene sediment deposition, and has been demonstrated in seismic and outcrop studies on the continental shelves of many margins, few or no seismic stratigraphic studies have investigated orbital forcing on deep-water sediment records. In this study, we combined detailed seismic stratigraphy and 3D geomorphological analysis of a high-resolution 3D seismic block in a detailed study of the stratigraphic evolution of the western Niger Delta intraslope basins over the last 5.5 Ma. Two mega seismic units named MSU 1 and MSU 2 were identified.

The change in sedimentary architecture from (i) mass flows and turbidite sequences to (ii) hemipelagic and turbidite sequences at the MSU 1/MSU 2 transition coincides with a significant (x3) increase in sedimentation rates and a transition from dominant 400 ka eccentricity cycles (from 5.3 Ma-0.8 Ma) to dominant 100 ka eccentricity cycles, at the Middle Pleistocene Transition (MPT) (circa 0.8-0 Ma). The timing of these changes was estimated based on a detailed analysis of seismic facies succession, correlation of seismic markers with high-resolution sea-level and oxygen isotope curves, and estimation of sequence duration. Further changes in the sedimentary record, characterised by turbidite dominated sequences at the lower part of MSU 1 to mixed mass flows and turbidite sequences at the upper part of MSU 1, were respectively correlated with changes that occurred in the early Pliocene (circa 4.9 Ma) and in the early Pleistocene (circa 2.6 Ma).

The depositional sequence on the western Niger Delta intraslope basin is usually characterised by a falling stage erosional surface (FSES) at its base and top (sequence boundary), and by (i) basal MTDs/bypass facies (where preserved), (ii) turbidite feeder channels/aggrading or meandering channel levee complexes and/or MTDs (slides/slumps) and (iii) hemipelagic drapes that successively document the falling stage, lowstand to early transgressive and late transgressive to highstand transits of the shoreline.

This seismic stratigraphic study demonstrates for the first-time sequence cyclicity associated with orbital (Milankovitch) forcing in the deep-water Niger Delta over the last 5.5 Ma. The Pliocene and Pleistocene sedimentary records of the western Niger Delta intraslope basins were controlled by interplay between allocyclic forcing linked to glacio-eustatic sea-level oscillations and basin tectonics associated with mobile shale movements, the latter being more prevalent from the early Pliocene to the MPT.

If calibrated with high-resolution biostratigraphic data in future studies, this study could serve as a useful analogue for further studies in the Gulf of Guinea, equatorial Atlantic and other margins fed by large deltas.

Keywords: Niger Delta; Intraslope basins; Pliocene; Pleistocene; Seismic stratigraphy; Allocyclic forcing; Eccentricity cycles.[1]

1. Introduction

Deep-water sediments are important archives of the Earth's history not only because they record past climatic, geodynamic, environmental and hydrodynamic changes (e.g. Burbank,1992; Molnar, 2004; Catuneanu, 2006; Posamentier and Kolla, 2003; Clift, 2010; Zecchin and Catuneanu, 2010), but also because they host viable hydrocarbon fields (see review in Morley *et al.,* 2011). Understanding the complex interplay between allocyclic (e.g. eustasy, tectonics, climate and indirectly sediment supply), and autocyclic (e.g. channel avulsion) or regional forcings (e.g. delta lobe switching, shale tectonics etc.), is critical for interpretation of the evolution of deep-water sedimentary systems (e.g. Elliot, 1975; Jervey, 1988; Posamentier *et al.,* 1988; Pulham, 1989; Linselle, 1991; Wiener *et al.,* 2010; Miall, 2010; Morley *et al.,* 2011; Catuneanu and Zecchin, 2013).

The Pliocene and Pleistocene are ideal time intervals for this kind of study because eustasy and climate proxies ($\delta^{18}O$) are well constrained and show significant variations both in amplitude and frequency (e.g. Ruddiman *et al.,* 1989; Imbrie *et al.*, 1993; Bassinot *et al*., 1994;

[a,b*] Corresponding autho :: Kelvin Ikenna Chima; Sorbonne Université; *Institut des Sciences de la Terre* (*ISTeP*), Case 129, Tour 56/66, fifth floor, 4 Place Jussieu, 75252, Paris Cedex. E-mail; kelvin.chima@sorbonne-universite.fr; kelvini.chima@gmail.com

Leroy *et al*., 1999; Shackleton, 2000; Lisiecki and Raymo, 2005; Miller *et al*., 2005; Gibbard *et al*., 2010; Gibbard and Lewin, 2016; Raymo *et al.,* 2018). Published climate proxies across the worlds' ocean basins show that the Pliocene and Pleistocene were controlled by orbital forcing (Milankovitch cycles) of three major periods namely: (i) precession (23 ka), (ii) obliquity (41 ka), and (iii) eccentricity (400 ka and 100 ka) (Lisiecki and Raymo, 2007). The early Pliocene from (5.3 Ma) to the early Pleistocene was dominated by obliquity cycles (41 ka), while the middle Pleistocene (circa 1.4 Ma) to the present was dominated by eccentricity (400 to 100) (Head and Gibbard, 2015a, b; Gibbard and Lewin, 2016). Although the switch to the eccentricity cycles is poorly understood and a transition period from 1.4 to 0.4 Ma was suggested by Head and Gibbard (2015a, b), and Gibbard and Lewin (2016), a marked change to increasingly severe glacial cycles, the so-called '0.8 Ma event' (Lisiecki and Raymo, 2007; Head and Gibbard, 2015a, b) or '0.9 Ma' (Miller *et al.,* 2005; Elderfield *et al.,* 2012), is usually interpreted as the Middle Pleistocene Transition (MPT).

Sedimentary records all over the world show the imprint of tectonic, climatic and glacio-eustatic cycles of different orders (Haq *et al.,* 1987). Fourth-order climate cycles lasting 400 ka have been reported during the Pliocene e.g. on the continental shelf offshore Foz do Amazonas Basin (Brazil), with incised valleys, slope canyons and mass wasting (Gorini *et al.,* 2014). During the Pleistocene, fifth-order glacio-eustatic sea-level changes with 100 ka periodicity are also well documented with marked shoreline progradation on the shelf and increased deep-water sedimentation during glacials e.g. in the Mediterranean Sea over the last 500 ka (Rabineau *et al.,*2006; Ridente *et al.,* 2008; Lafosse *et al.,* 2018). During the Pliocene, sediment architecture in the Mediterranean Sea does not appear to be much imprinted by the 400 ka cycles as shown in seismic (Rabineau *et al.,* 2014) and numerical simulations (Leroux *et al.,* 2014), probably

because of an anomaly in accommodation created by the erosion of the entire margin after the Messinian Salinity Crisis. 100-ka glacio-eustatic cycles have also been described worldwide e.g. offshore Alaska (Gulick *et al.,* 2012), in the Gulf of Mexico (Galloway, 2001) and the Bengal fan (Werber *et al.,*1997).

In the eastern Niger Delta, Jermannaud *et al.* (2010) and Rouby *et al.* (2011), documented a transition from global climate-controlled sequences from circa 4-2.5 Ma to sediment supply-controlled sequences from 2.5 Ma to the present. These authors also demonstrated a general progradation and an increase in sedimentation rates from 4-2.5 Ma, followed by a retrogradation and a decrease in sedimentation rates over the last 2.5 Ma. Additionally, Riboulot *et al.* (2012), showed that eccentricity forcing of 100 ka periodicities has controlled the stratigraphic evolution of the eastern Niger Delta continental shelf over the last 0.5 Ma.

In the western Niger Delta slope, where the present study was conducted (Fig. 1), Jobe *et al.* (2015, 2016; red box in Fig. 1A, D), linked changes in sedimentation rates during the last 130 ka (MIS 5e to the present) to glacial/interglacial cycles with increased sedimentation rates during the lowering of the sea level (MIS3 and MIS2) and an overall reduction in sedimentation during a rapid post-glacial sea-level rise associated with the Meltwater pulse 1A at 14 ka. Earlier studies e.g. Lézine et *al.* (2005); Weldeab *et al.* (2011); Collins *et al.* (2014); Govin *et al.* (2014) and Armitage *et al.* (2015), linked the increase in sedimentation rates in the Gulf of Guinea during the Quaternary to the West African Monsoon. A recent high-resolution, 3D seismic and sequence stratigraphic study of the western Niger Delta slope (yellow box in Fig. 1A, C, D, E) by Chima *et al*. (2019, dated the Neogene stratigraphic record from the Burdigalian (18.5 Ma) to the late Miocene (5.5 Ma), and described interactions between mobile shale and erosional submarine channel over the last 5.5 Ma. However, the lack of biostratigraphic data for the Pliocene and

5

Pleistocene poses a challenge to constraining the timing of major changes in sedimentary records.

Despite the above-mentioned studies of the Pliocene and Pleistocene sedimentary records in the Niger Delta, no study has investigated its control by orbital forcings from the late Messinian (5.5 Ma) to the present. Hence, the objective of this paper is to perform a detailed analysis of the stratigraphic evolution of the western Niger Delta intraslope basins over the last 5.5 Ma with a view to (i) proposing a sequence stratigraphic framework for the Pliocene and Pleistocene intervals; and (ii) investigating their control by orbital forcings.

The Niger Delta is an ideal laboratory to study climate stratigraphy and slope depositional processes because it is located on a passive margin where the imprints of regional/global climate dynamics, sea-level variation, gravity-tectonics, drainage evolution and sediment supply are well imaged on high-resolution 3D seismic reflection data.

2. Regional Setting

The Cenozoic Niger Delta is located in the Gulf of Guinea on the equatorial Atlantic margin of West Africa (Fig. 1A). The delta is the twelfth largest petroleum province in the world (Tuttle *et al.,* 1999). It covers an area of ~140,000 km^2 with a maximum sediment thickness of ~ 12 km (Allen, 1965; Evamy *et al.,* 1978; Doust and Omatsola, 1990). The Niger Delta is divided into the Eastern and the Western lobes by a Cretaceous basement high [the Charcot Fracture Zone (CFZ)] (Corredor *et al.,* 2005; Fig. 1A). The development of the delta since the late Eocene (Fig. 1B, C), has led to three major structural zones:(i) an extensional zone (EZ) below the continental shelf characterised by normal faults; (ii) a translational zone (TZ) below the upper slope dominated by mobile shales and intraslope basins, and (iii) a contractional zone (CZ)

located at the toe of the slope characterised by reverse faults and detachment folds (Doust and Omatsola, 1990; Damuth, 1994; Cohen and McClay, 1996; Connors *et al.,* 1998; Morgan, 2004; Bilotti *et al.*, 2005; Corredor *et al.,* 2005; Fig. 1A, C).

The classification scheme of Prather *et al.* (2003) describes the western Niger Delta slope profile as a 'graded slope' characterised by a seafloor whose downslope profile is elevated above the level of theoretical concave-upward, smoothed graded profile. Shale tectonics on the Niger Delta slope give rise to shale/thrust-cored structural highs flanked by mobile shale withdrawal intraslope basins that interact with sediment-gravity flows (Doust and Omatsola, 1990; Damuth, 1994; Cohen and McClay, 1996; Connors *et al.,* 1998; Graue, 2000; Morgan, 2004; Bilotti *et al.*, 2005; Corredor *et al.,* 2005; Wiener *et al.,* 2010; Prather *et al.,* 2012; Fig. 1D, E). The western Niger Delta slope is in constant dynamic equilibrium as the movements of mobile shale create structural highs which, in turn, are smoothed by sediment-gravity flows that preferentially accumulate within adjacent intraslope basins (Deptuck *et al.,* 2003; Adeogba *et al.,* 2005; Bakare *et al.,* 2007; Prather *et al.,* 2012; Clark and Cartwright, 2012; Chima *et al.,* 2019; Fig. 1D, E). The distribution of shale/thrust-cored structures on the western Niger Delta slope significantly controls the morphology of submarine channels, depositional patterns, reservoir architecture and distribution (e.g. Adeogba *et al.,* 2005; Bakare *et al.,* 2007; Jobe *et al.,* 2015, 2016; Clark and Cartwright, 2012; Deptuck *et al.,* 2012; Prather *et al.,* 2012; Jolly *et al.,* 2016; Hansen *et al.,* 2017; Chima *et al.,* 2019). The present study was conducted in the translational zone of the western Niger Delta slope at the transition between the extensional and the contractional domains (Fig. 1A, C). The study area covers 638 km^2 at ~120 km from the present-day coastline and lies at water depths ranging from 900 to 1,755 m (Fig. 1E).

3. Dataset and Methods

3.1 Dataset

We used high-resolution 3D seismic data and lithologic logs from five boreholes (see Fig. 1A, D, E), to study the Pliocene and the Pleistocene stratigraphic evolution of the western Niger Delta.

3.1.1 Seismic data

The 3D seismic data was processed as a zero-phase source wavelet in the American reverse standard polarity such that an increase in acoustic impedance corresponds to a trough (blue loop) in the wavelet, while a decrease in acoustic impedance is represented by a peak (red loop) in the wavelet. The horizontal resolution of the data is characterised by a stacking bin spacing of 25 m x 25 m (inline and crossline spacing), and a seismic recording sampling interval of 4 milliseconds two-way travel time (TWT). The dominant frequency of the data is 30 Hz over the first 3 seconds (TWT), which yields a vertical resolution of ~13.7 meters within the interval of interest.

3.1.2 Well data

The well data comprise gamma-ray logs from five wells (labelled W1, W2, W3, W4 and W5 in Fig. 1A, D, E). Wells W2-W5 penetrate only the lower part of the Pliocene whereas W1 covers the Neogene to the late Pleistocene (see Figs. 2; 7 and 9B of Chima *et al.,* 2019). The most recent available biostratigraphic dating corresponds to the late Messinian (circa 5.5 Ma), based on the last recorded occurrence of *Discoaster quinqueramus* (see Chima *et al.,* 2019).

Biostratigraphic data were not available for the interval of interest (the Pliocene and the Pleistocene).

3.2 Methods

3.2.1 Seismic stratigraphy

We applied the concept of seismic stratigraphy (after Mitchum and Vail, 1977) to analyse the sedimentary architecture of the Pliocene and Pleistocene sedimentary records of the western Niger Delta intraslope basins. Our seismic stratigraphic approach relied on the recognition of reflection amplitude, continuity, internal architecture, external geometry, the nature of bounding surfaces and erosional truncations to delineate key seismic surfaces as well as their association with seismic facies.

3.2.2 3D seismic geomorphology

We applied the 3D seismic geomorphological analysis technique described by Posamentier and Kolla (2003) and Catuneanu (2006) for our detailed study of the depositional environments corresponding to the seismic facies described above. This was achieved by detailed analysis of root mean square (RMS) seismic amplitudes, that makes it possible to distinguish lithological and depositional environments (see Chima *et al.,* 2019; and references therein). Analyses of the RMS amplitudes were combined with variance seismic attributes to guide the geological interpretation of the seismic data (Chopra and Mafort, 2007; Taner *et al;* 1994; Chima *et al.,* 2019). Three (3D) seismic geomorphological analyses enabled the detailed study of the space-time evolution of the Pliocene and the Pleistocene sedimentary records.

3.2.3 Allostratigraphic partitioning and dating of the Pliocene and the Pleistocene stratigraphy

Detailed analysis of RMS maps combined with variance analysis of seismic attributes and 3D geomorphological interpretation of the seismic data made it possible to define 21 mappable seismic surfaces, which bound the fourth-and fifth-order allostratigraphic sequences as defined by Catuneanu (2006) and Catuneanu *et al.* (2011). These allostratigraphic units were grouped in two mega seismic units (MSU 1 and MSU 2). As no biostratigraphic data were available for the Pliocene or the Pleistocene, we used the most recent biostratigraphically constrained interval (the late Messinian) dated at ~5.5 Ma based on the last recorded occurrence of *Discoaster quinqueramus* (see Chima *et al.*, 2019), to define the age of the lower part of MSU 1. Then, we matched the key erosional and conformable seismic surfaces that show significant changes in the sedimentary architecture both in seismic lines and on 3D geomorphological maps with the high-resolution Pliocene and the Pleistocene sea-level and oxygen isotope (^{18}O) curves derived from (Lisiecki and Raymo, 2005; Raymo *et al.*, 2018).

4. Results and Interpretations

4.1. Seismic facies analysis

The Pliocene and Pleistocene stratigraphy of the western Niger Delta intraslope basins were subdivided into two mega seismic units named MSU 1 and MSU 2, based on the observed changes in seismic geometries and depositional environments. MSU 1 and MSU 2 correspond to Unit 6 and Unit 7 respectively in Chima *et al.* (2019). Although a detailed seismic facies analysis of the study area was presented in Chima *et al.* (2019) (Fig. 1A, C, D, E; 2A), the present study sheds more light on facies association and improves our understanding of depositional processes

and sequence stratigraphy in a deep-water (slope) setting. The six seismic facies previously described in the study area by Chima *et al.* (2019) include: (1) chaotic, discontinuous low-amplitude (B_l) seismic facies, characterised by elongate/tabular geometry, irregular tops and erosional bases, interpreted as mass-transport deposits (MTDs; Fig. $2A_1$, B, C); (2) chaotic, discontinuous to moderately continuous, high-amplitude (B_h) seismic facies, characterised by irregular base, blocky external form and sinuous planform geometry, interpreted as turbidite feeder channels/aggrading or meandering channel levee complexes (CLCs; Fig. $2A_2$, B); (3) coherent/slightly inclined, moderate to high-amplitude seismic facies that generally border the margins of concave-upward negative relief and display tortuous planform geometry, interpreted as MTDs (slides/slump blocks?; Fig. $2A_3$); (4) parallel continuous to slightly convergent, high-amplitude, (C_{bh}) seismic facies that display fan shaped geometry with high RMS amplitude on the map, interpreted as distributary channels/lobes ($2A_4$, C); (5) convergent/thinning, high-to moderate-amplitude, (C_{th}) seismic facies, characterised by wedge geometry, which borders negative relief, marked by sinuous planform geometry, interpreted as channel levee deposits ($2A_5$, B, C); (6) transparent, parallel, continuous, draping seismic facies (D) that locally display small-scale chaotic internal architecture, bounded by conformable surfaces interpreted as hemipelagic drapes and/or muddy turbidites ($2A_6$, B, C). The foregoing seismic facies and their interpretations were confirmed by 3D seismic geomorphology (Figs. 3-10) and are consistent with previous studies of the Niger Delta intraslope basins (e.g. Deptuck *et al.,* 2003; 2012; Adeogba *et al.,* 2005; Bakare *et al.,* 2007; Hansen *et al.,* 2017).

4.2 Facies association

Seismic facies on the western Niger Delta intraslope basins display complex lateral and vertical arrangements inside and outside erosional submarine channels MSU 1 and MSU 2 (e.g. Fig. 2A, B, C).

4.2.1 Association of seismic facies in mega seismic unit 1 (MSU 1)

In MSU 1, we observed a 2.5 km wide concave-upward negative topography (185 m deep) that obstructs the lateral continuity of seismic reflections (e.g. Fig. 2B). Within this topographic feature, a narrow (1 km wide, 90 m deep), vertically stacked, concave-upward negative topographies were also observed (e.g. Fig. 2B). The 2.5 km and the 1 km wide negative topographies were interpreted as, respectively, erosional submarine channels and channel levee systems (CLSs) or channel forms (after Deptuck et $al.$ 2003; e.g. Fig. 2B).

4.2.1.1 Association of seismic facies within the erosional submarine channels in MSU 1

The association of facies within the erosional submarine channels in MSU 1 includes: (i) B_l seismic facies (MTDs), named basal MTDs; (ii) B_h seismic facies, which correspond to turbidite feeder channels/aggrading or meandering channel levee complexes, and (iii) C_{th} seismic facies, which correspond to channel levee deposits (e.g. Fig. 2A, B). Levee deposits were further subdivided into inner and outer levee (IL and OL) deposits, respectively, depending on whether sedimentation occurred inside or outside the erosional submarine channel (e.g. Fig. 2B). These B_l, C_{th} and the B_h seismic facies generally infilled erosional submarine channels in MSU 1 (e.g. 2B). Each erosional submarine channel and associated infilling was generally abruptly overlain by another negative topography (erosional submarine channel) with or without complete

preservation of the B_l, C_{th} and the B_h seismic facies (Fig. 2B). The entire system is locally overlain by another B_l seismic facies (MTD; e.g. Fig. 2B).

4.2.1.2 Association of seismic facies outside the erosional submarine channels in MSU 1

Outside the erosional submarine channels in MSU 1, seismic facies generally stack vertically from (i) B_l facies (basal MTDs), (ii) the C_{th} facies (channel levee deposits), (iii) the B_l facies (MTDs), (iv) the C_{bh} facies (distributary channels/lobe deposits) and the D seismic facies (hemipelagic drape) (e.g. Fig. 2C). The B_l seismic facies (MTDs) generally disrupt the lateral continuity of the underlying C_{th} seismic facies (e.g. 2C).

4.2.2 Association of seismic facies in MSU 2

In MSU 2, similar concave upward negative topographies previously described and interpreted as erosional submarine channels and CLSs (Fig. 2B), were also observed in MSU 2 (e.g. Fig. 3A, B). How the seismic facies are associated inside and outside the erosional submarine channels is described below.

4.2.2.1 Association of seismic facies within the erosional submarine channels in MSU 2

In MSU 2, the seismic facies in the erosional submarine channels generally stack from (i) the B_h facies (turbidite feeder channels/aggrading or meandering channel levee complexes); (ii) coherent/slightly inclined, moderate to high amplitude seismic facies that generally border the margins of concave-upward negative relief and display tortuous planform geometry (slide/slump blocks) (Fig. 2A; 3A, B) to (iii) the D facies (hemipelagic drape), where preserved (e.g. horizons S and X in Fig. 3A, B). The coherent/slightly inclined, moderate to high amplitude seismic facies

13

(slide blocks/slump deposits) locally disrupt the lateral continuity of the underlying B_h seismic facies (e.g. Fig. 3A, B).

4.2.2.2 Association of seismic facies outside the erosional submarine channels in MSU 2

In MSU 2, the association of seismic facies outside erosional submarine channels includes: (i) the C_{th} facies (aggrading channel levee/overbank deposits); (ii) the B_l facies (MTDs), and (iii) the D facies (hemipelagic drape) (see the stratigraphic interval between horizons T and V at the extreme left in Fig. 3A, B). As observed in MSU 1, the B_l facies (MTDs) generally disrupt the lateral continuity of the C_{th} seismic facies (e.g. Fig. 3A, B).

4.3 3D seismic geomorphology and sedimentary architecture

A total of 21 seismic surfaces (13 in MSU 1, labelled M-P) and (8 in MSU 2, labelled Q-X in Figs. 3-10), were analysed in detail in this study. Only a few representative erosional surfaces in the lower, middle, and upper parts of MSU 1 and MSU 2 which illustrate the main changes in the sedimentary architecture of the Pliocene and the Pleistocene are presented here.

4.3.1 Base of MSU 1 (horizon M)

Description

The base of MSU 1 (horizon M in Fig. 3B) is unerlain by > 80 m thick transparent, parallel continuous, D seismic facies (highlighted in blue in Fig. 3B). The M horizon is traceable through a significant part of the study area except across the overlying 185 m negative relief (horizon A in Fig. 3A) and the mounded seismic wipe out zone in the northern part of the study area (Figs. 1D, 3A, B). The 185 m deep relief associated with horizon A marks the onset of the

14

chaotic, discontinuous low amplitude (B_l seismic facies), the convergent/thinning, high to moderate amplitude (C_{th} seismic facies) and the parallel continuous to slightly convergent, high amplitude (C_{bh} seismic facies) (Fig. 3A, B). An RMS amplitude map draped on a variance attribute of the 185 m deep relief associated with horizon A, shows the presence of a 1.5 km wide, east-west trending, relatively straight planform feature (labelled 1 in Fig. 3C), and two narrow winding features (labelled 2, 3 in Fig. 3C), in the southern part of the study area. The narrow winding feature (labelled 2 in Fig. 3C), is connected to a fan-shaped feature to the southwest. Linear scars with respectively, northeast-southwest, radial, and east-west orientations, are observed in the northern, central, and southern parts of the study area (Fig. 3C). A grey area (dashed red line) is observed in the north-eastern part of the study area characterised by radial features at its southern tip (Fig. 3C). The narrow winding feature (labelled 3 in Fig. 3C), crosses an oblique, elongated positive relief to the south. A north-south seismic line (CC^I), (located in Fig. 3C), illustrates the sedimentary architecture of horizon A (Fig. 3A, B). Northeast-southwest trending linear scars generally offset stratigraphy normally except in the north, where one of the scars (labelled Z in Fig. 3B) offsets stratigraphy normally at its lower part but inversely at its upper part.

Interpretation

The >80 m thick transparent, parallel continuous, draping seismic unit, characterised at the base by a conformable seismic surface (labelled horizon M in Fig. 3B), corresponds to the hemipelagic drape (HD)/muddy turbidites, dated at 5.5 Ma (see Chima *et al.,* 2019). The conformable nature of this hemipelagic drape suggests that it passively draped the slope during the episode of maximum flooding of the continental shelf and sediment starvation in the deep

basin (see Chima *et al.,* 2019; and references therein). This interpretation is supported by the fact that the *D. quinqueramus* (calcareous nannofossil) we used in dating the hemipelagic drape at 5.5 Ma is globally recognised as an important marker of the high sea level in the late Miocene (e.g. Backman *et al.,* 2012). The 1.5 km wide and 185 m deep negative relief associated with horizon A (Fig. 3B), which displays straight planform geometry (Fig. 3C), corresponds to the erosional submarine channel described in section 4.2.1. The lateral discontinuity of horizon M (the base of the hemipelagic drape dated at 5.5 Ma) caused by the overlying horizon A, further supports the interpretation of the latter as an erosional surface (Fig. 3B). The b_l, C_{th} and the C_{bh} seismic facies that generally overlie horizon A correspond to, respectively, the MTDs, channel levee deposits/CLSs and the turbidite feeder channels/aggrading, or meandering channel levee complexes described above (Figs. 2A, B; 3A, B). The narrow, winding features (labelled 2, 3) south of the main erosional submarine channel in Fig. 3C, were interpreted as sinuous channel levee systems (CLSs) or channel forms (after Deptuck *et al.,* 2003; Fig. 3C). The fan-shaped feature associated with CLS 2 was interpreted as a transient fan/lobe deposit (after Adeogba *et al.,* 2005; Fig. 3C). The seismic wipe out/grey area in the north-eastern part of the study area was interpreted as a mobile shale, while the linear scars and oblique/elongated feature, crossed by a CLS to the south, were respectively interpreted as normal faults and buried folds (see Chima *et al.,* 2019; Fig. 3C). The change in the stratal offset patterns along fault Z (Fig. 3B), from normal at the lower stratigraphic level to inverse at the upper stratigraphic level, was interpreted as fault inversion linked to shale tectonics.

4.3.2 Middle part of MSU 1 (horizons G and I)

Description

An RMS amplitude map of horizon G draped on the variance attribute extraction in the middle part of MSU 1 (horizon G), reveals the presence of four narrow, winding features (labelled 1a, 2, 3 and 4 in Fig. 4A) located in the north-western and south-eastern parts of the study area. Compared to winding features 1a and 4, features 2 and 3 display elongated borders of moderate RMS amplitudes (Fig. 4A). Linear scars display trends that vary with the northeast-southwest and east-west orientations, dominate the northern part of the study area, while the radial patterns dominate the central part of the study area (Fig. 4A). A NE-SW grey area subdivides the study area into northern and southern halves (Fig. 4A). An irregular, rounded, chaotic area is visible in the SE corner of the study area (dashed black line in Fig. 4A). A seismic line (DD^I) through the winding features 1a and 2, reveals the presence of a 1 km wide, 120 m deep relief, infilled with the chaotic, discontinuous to moderately continuous, high amplitude, B_h and convergent/thinning, high to moderate amplitude, C_{th} seismic facies that also infill erosional channels 1a and 2 (Fig. 4B).

Furthermore, a variance attribute extraction on the horizon I, in the middle of MSU 1 (above horizon G), reveals the presence of a 2.5 km wide, sinuous feature (labelled 1b) to the north, characterised by the presence of narrower, winding features in its central part (Fig. 5A). A chaotic area is visible on the outer side of the main sinuous feature to the northeast, which is characterised by smaller, linear or slightly curved features (Fig. 5A). A seismic line (BB^I) crossing the main sinuous feature (Fig. 5A) reveals the presence of a 176 m deep relief corresponding to horizon I (Fig. 5B). The 2.5 km wide negative relief associated with horizon I and the enclosed narrower sinuous features are infilled with the chaotic, discontinuous low amplitude, B_l seismic facies, the convergent/thinning, high to moderate amplitude, C_{th} seismic facies and the parallel continuous to slightly convergent, high amplitude, C_{bh} seismic facies that

17

generally disrupt the lateral continuity of the underlying B_l and the C_{th} seismic facies (Fig. 5B). These seismic facies are unconformably overlain by a negative relief corresponding to horizon J (Fig. 5B). In turn, horizon J is overlain by a 166 m deep narrow relief, infilled with the chaotic, discontinuous to moderately continuous, high amplitude B_h seismic facies, bordered by the convergent/thinning, high to moderate amplitude C_{th} seismic facies (Fig. 5B). The entire system is abruptly overlain by the chaotic, discontinuous low amplitude, B_l seismic facies, covered by hemipelagic drape and display an overall convex-upward geometry (Fig. 5B).

Interpretation

The four narrow winding features associated with horizon G in (Fig. 4A) were interpreted as CLSs or channels forms, while the moderate amplitude zones that parallel the borders of the CLSs 2 and 3 were interpreted as channel belts (Fig. 4A). The NE-SW oriented grey area/seismic wipe-out zone corresponds to the area affected by mobile shale and/or erosion (Fig. 4A). The irregular chaotic area in the SE corner of the study area was interpreted as MTD (Fig. 4A). The 1 km wide, 120 m deep relief associated with horizon G was interpreted as erosional CLS (Fig. 4B). The chaotic, discontinuous to moderately continuous, high amplitude, B_h seismic facies and the convergent/thinning, high to moderate amplitude, C_{th} seismic facies that respectively infill and border the erosional CLS associated with horizon G, were interpreted as turbidite feeder channels/aggrading or meandering channel levee complexes and outer levee deposits. The presence of the C_{th} seismic facies (OL) deposits at nearly the same stratigraphic level as the infill of the erosional CLSs (labelled 1a in Fig. 4B), suggests that sediment-gravity flows within the channel were unconfined (see Deptuck *et al.,* 2003; Fig. 4B).

18

The 2.5 km wide, sinuous feature associated with horizon I (Fig. 5A) was interpreted as a sinuous, erosional submarine channel/erosional surface, while the smaller winding features within the erosional channel were interpreted as CLSs (Fig. 5B). The chaotic, discontinuous low amplitude, B_l seismic facies, the convergent/thinning, high to moderate amplitude, C_{th} seismic facies and the parallel continuous to slightly convergent, high amplitude, C_{bh} seismic facies that infill or border the erosional submarine channel and the channel forms were interpreted, respectively, as MTDs, channel levee deposits, and distributary channels/lobes (Figs. 2B, 5B). While the convergent/thinning, high to moderate amplitude. C_{th} seismic facies, confined to the main erosional submarine channel (horizon I) was interpreted as inner levee (IL), the C_{th} seismic facies on the outer bank of the erosional channels were interpreted as outer levee (OL) deposits (Figs. 2B, 5B). The presence of the IL deposit to the right of the main erosional submarine channel, coupled with the narrowing and lateral shifts of the enclosed CLSs/channel forms (red arrow in Fig. 5B), were interpreted as recording different stages of meandering/lateral aggradation of the system. The presence of OLs at every stage of the erosional submarine channel (Fig. 5B), suggests that sediment-gravity flows were not confined during the development of the system. The convex-upward geometry, displayed by the entire system, suggests that it was overfilled.

4.3.3 Upper part of MSU 1 (horizon K)

Description

An RMS amplitude map draped on a variance attribute extraction in the upper part of MSU 1, (labelled horizon K in Fig. 6A), reveals the presence of a 1.8 km wide, bifurcating planform feature in the northern part of the study area (labelled 1c in Fig. 6A). The feature

displays an overall moderate RMS amplitude and is characterised by smaller, winding features with higher RMS amplitude (Fig. 6A). A linear relief is visible on the outer bend of the main system (Fig. 6A). A north-south seismic line (FF^{I}) through the centre of the system reveals a 1.8 km wide, 90 m deep negative relief, infilled with the chaotic, discontinuous to moderately continuous, high amplitude, B_h seismic facies (Fig. 6B). The B_h seismic facies is unconformably overlain by the chaotic, discontinuous low amplitude, B_l seismic facies, covered by hemipelagic drape and display an overall convex-upward geometry (Fig. 6B).

Interpretation

The 1.8 km wide, 90 m deep relief, characterised by moderate RMS amplitudes and the enclosed, narrow winding features that display higher RMS amplitudes were interpreted as an erosional submarine channel and CLSs, respectively (Fig. 6A, B). The chaotic, discontinuous to moderately continuous, high amplitude, B_h seismic facies which infill the erosional submarine channel were interpreted as turbidite feeder channels/aggrading or meandering channel levee complexes, while the overlying, unconformable, B_l seismic facies were interpreted as MTDs (Fig. 5B). The sharp relief at the outer bend of the erosional submarine channel was interpreted as a terrace (Fig. 6A, B). The fact this feature matches the earlier erosional submarine channels (labelled 1a-c in Figs. 4A, 5A and 6A), suggests that the feature has been active since the time equivalent to horizon E (Fig. 4A). Between the early stage (labelled 1a in Fig. 4A) and the late stage (labelled 1c in Fig. 6B), this erosional channel migrated more than 10 km NW-SE, with an overall increase in width and erosional efficiency until the age equivalent to that of horizon K, when it was truncated by the overlying, B_l seismic facies (MTDs; Fig. 6B). The convex-upward geometry, displayed by the entire system, suggests that it was overfilled.

4.3.4 Base of MSU 2 (horizon Q)

Description

An RMS amplitude map at the base of MSU 2 draped on a variance attribute map (the horizon labelled Q in Fig. 3B), reveals the presence of a 2.5-km wide, sinuous NE-SW trending feature and smaller, NE-SW winding features (labelled 1, 2, 3 and 4, respectively, in Fig. 3D), all in the southern part of the study area. In the northern part of the study area, linear scars display east-west, northeast-southwest and radial patterns from the distal central to proximal parts, respectively (Fig. 3D). Towards the northeast, two large dark rounded features (>1.5 km wide), characterised by low RMS amplitudes are flanked by smaller, dark rounded features (Fig. 3D). The large, dark rounded feature to the extreme north-east is marked at its centre by a 0.3 km wide, rounded feature (Fig. 3D). In the north-western part of the study area, a 1 km wide sinuous feature highlighted in grey, marks the northern limit of the small, dark rounded features (Fig. 3D). A north-south seismic line (CC') crossing these features, illustrates their stratigraphic architecture (Fig. 3A, B).

Interpretation

The 2.5 km wide, NE-SW trending feature (labelled 1 in the southern part of Fig. 3B, D) and the sinuous feature highlighted in grey to the northwest, correspond to the eroded portion of the stratigraphy, while the narrow winding features (labelled 2, 3 and 4 in Fig. 3D) were interpreted as CLSs. The east-west and northeast-southwest trending as well as radial scars (Fig. 3D) that offset stratigraphy on seismic line (Fig. 3B), were interpreted as normal faults. The large and smaller, dark rounded features in the northern part of the study area were interpreted as mobile shales and fluid escape features, respectively (Fig. 3D). The 0.3 km wide, rounded

feature in the centre of the mobile shale to the northeast was interpreted as a giant pockmark (after Ribolout *et al.,* 2012).

4.3.5 Middle part of MSU 2 (horizon R)

Description

An RMS amplitude map in the middle of MSU 2 superimposed on a variance attribute extraction (the level of horizon R in Fig. 7C) reveals the presence of a NE-SW trending, 2.5 km wide sinuous feature, with low RMS amplitude (Fig. 7A, B). This sinuous feature increases in width downstream to the southwest and is characterised by many smaller winding features within the main system (Fig. 7A, B). Rounded relief features > 300 m wide are present on the middle outer bend of the system (Fig. 7A, B). Three narrow winding features are observed south of this sinuous feature, (Fig. 7A, B). Radial, NE-SW and E-W trending linear scars occur in the north, central and southern parts of the study area, respectively (Fig. 7A, B). To the north, two rounded, dark features with low RMS amplitudes are observed associated with the lower feature, flanked by smaller rounded, dark features which are confined within the NE-SW and E-W trending linear scars (Fig. 7A, B). A north-south seismic line (GG^I) through the main sinuous feature, reveals the presence of a 185-m deep, negative relief, characterised by elevated margins and irregular scars to the right of the feature (Fig. 7C, D, E). The 185-m deep relief is infilled with chaotic, discontinuous to moderately continuous, high amplitude, B_h seismic facies, which in turn, are unconformably overlain by the coherent/slightly inclined, moderate to high amplitude seismic facies (Fig. 7C, D, E). The infill of the relief associated with horizon R is unconformably overlain by a 180 m relief and a 100 m deep relief that correspond, respectively, to horizons V and W (Figs. 7C, D, E; 8D, E). These topographies are in turn infilled with chaotic,

discontinuous to moderately continuous, high amplitude, B_h seismic facies and coherent/slightly

inclined, moderate to high amplitude seismic facies (Fig. 7C, D, E). The entire system is overlain

by an irregular seismic reflection (horizon X), which, in turn, is covered by transparent, parallel

continuous, D seismic facies (Fig. 7C, D, E).

Interpretation

The 2.5 km wide, 185 m deep sinuous feature, associated with horizon R was interpreted

as a sinuous erosional submarine channel (Fig. 7A-E). The chaotic, discontinuous to moderately

continuous, high amplitude, B_h seismic facies and the coherent/slightly inclined, moderate to

high amplitude seismic facies that infill the erosional channels/erosional surfaces associated with

horizons R, V and W (Fig. 7A-E) were interpreted as turbidite feeder channels/aggrading or

meandering channel levee complexes and MTDs (slides/slump blocks?), respectively. These

turbidite feeder channels/aggrading or meandering channel levee complexes resemble the highly

incisional, high amplitude reflections (HARS) previously described on the western Niger Delta

slope (e.g. Deptuck *et al.,* 2003, Heiniö and Davies, 2007; Hansen *et al.,* 2017) and elsewhere on

the adjacent side of the equatorial Atlantic, the Rio Muni Basin (Equatorial Guinea) (see Jobe *et

al.,* 2011). The transparent, parallel continuous, D seismic facies, which drape the entire system

was interpreted as a hemipelagic drape (Fig. 7C-E). The > 300 m wide, rounded features on the

middle outer bend of the erosional submarine channel were interpreted as slides/slump scars

(Fig. 2A, 7A, B). The narrow, winding features to the south of the main erosional channel were

interpreted as sinuous CLSs or channel forms (see Deptuck *et al.,* 2003; Fig. 7A, B). The lateral

discontinuity of seismic reflections (e.g. the horizons P and Q) on the adjacent side of the

erosional channel (Fig. 7C-E), demonstrates the erosional character of the sediment-gravity

23

flows that sculpted the channel. This interpretation is supported by the channel's deeply incised nature (185-m deep) and the presence of terraces (multiple slide/slump scars) along the elevated margins of the channel (Fig. 7C-E). The relatively confined nature of the erosional submarine channels, the dominance of channel infills by turbidite feeder channels/aggrading or meandering channel levee complexes within the channels and the presence of MTDs (slides/slumps?), distinguish the submarine channels observed in MSU 2 from those observed in MSU 1, where the channels are generally unconfined (e.g. Figs. 4B, 5B). The vertical superposition of erosional submarine channels with minor lateral migration (Fig. 7C-E) demonstrates the complex cut and fill architecture of the system with overall vertical aggradation (red arrow in Fig. 7E). The radial, E-W and NE-SW trending linear scars distributed in the north, central and southern part of the study area, were interpreted as normal faults (Fig. 7A-C). The rounded, dark features with low RMS amplitudes were interpreted as mobile shales, while the smaller, dark rounded features that flank the mobile shales were interpreted as fluid escape features (Fig. 7A, B). These mobile shales, mud volcanoes, fluid escape features, BSR and pockmarks (Figs. 1E, 3A, 8A, 9A), support fluid overpressure in the study area (see also Riboulot *et al.,* 2011).

4.3.6 Upper part of the MSU 2 (horizons V and W)

Description

An RMS amplitude map of horizon V draped on a variance attribute extraction at the upper part of MSU 2 reveals the presence of a 2.1 km wide, sinuous planform feature, characterised by moderate RMS amplitudes and smaller winding features within the main system (Fig. 8A, B). Smaller winding features also occur in the northern and southern parts of the study area (Fig. 8A, B). The borders of the main sinuous system are irregular and contain some

24

detached curved loops at its outer bends (Fig. 8A, B). North of the system, a NE-SW trending, wedge-shaped chaotic area of low RMS amplitude is observed (dashed black lines in Fig. 8A, B). Further to the north of the study area, two rounded, dark features with low RMS amplitudes are associated with smaller, dark rounded features (Fig. 8A, B). Some of the smaller, dark rounded features are confined within the NE-SW trending short and long linear scars (Fig. 7A, B). A NW-SE seismic line (HH^I) illustrates a 105 m deep negative relief associated with the 2.1 km wide sinuous feature (Fig. 8C-E). This feature is infilled with chaotic, discontinuous to moderately continuous, high amplitude, B_h seismic facies which, in turn, are unconformably overlain by the coherent/slightly inclined, moderate to high amplitude seismic facies (Fig. 8C-E). The infill of the erosional channel/surface associated with horizon V is abruptly overlain by another 100 m deep relief associated with the overlying horizon W (Figs. 7C-E; 8C, 9A). The topographies of horizons V and W respectively disrupt the lateral continuity of the relatively thick, convergent/thinning, high to moderate amplitude, C_{th} seismic facies, the parallel continuous to slightly convergent, high amplitude, C_{bh} seismic facies, and the draping, D seismic facies (Fig. 7C, 8C). Towards the right of Fig. 8C, thin, laterally confined, somewhat coherent, low to moderate reflectivity seismic reflections overlie horizon V (above the V-shaped, linear scars, that offset seismic reflections in Fig. 8A-C).

An RMS amplitude map superimposed on a variance attribute map (the level of the horizon W), just above (the horizon V), reveals the presence of a 2.5 km wide, sinuous planform feature with low RMS amplitudes and characterised by narrow winding features (Fig. 9A). South of the main sinuous system, two elongate features, characterised by high RMS amplitudes in the eastern and western parts of the study area are observed, with narrow, winding features crossing the eastern elongate feature (Fig. 9A). To the north, two rounded, dark features are flanked by

25

short and long linear scars that are in turn, flanked by smaller, dark rounded features (Fig. 9A). An irregular chaotic area with an overall low RMS amplitude to the northeast (dashed black line in Fig. 9A), occurs adjacent to the rounded, dark features (Fig. 9A). An E-W oriented seismic line (JJ^{I}) which crosses the elongated features with high RMS amplitudes in the southern part of the study area, shows their high reflectivity and onlapping geometry at the margin of the intraslope basin (yellow arrow in the top left-hand corner of Fig. 9B). Although our observations of the previous seismic lines show that the infills of negative topographies are generally chaotic and difficult to trace (e.g. Figs. 3A, B, 7C, D), the erosional surfaces (labelled horizons X and W in Fig. 8C-E), were locally correlated inside the negative relief.

Interpretation

The wide sinuous features associated with horizons V and W (Figs. 8A, B; 9A) were interpreted as meandering, erosional submarine channels, while the narrow winding features to the north and south of these features were interpreted as sinuous CLSs or channel forms. (Figs. 8A, B; 9A, B). The chaotic, discontinuous to moderately continuous, high amplitude, B_h seismic facies and the coherent/slightly inclined, moderate to high amplitude seismic facies that infill the erosional submarine channels associated with horizons V and W were respectively interpreted as turbidite feeder channels/aggrading or meandering channel levee complexes and MTDs (?slide blocks/slump deposits) (Fig. 8A-E). The occurrence of the slide/slump deposits at the same stratigraphic level as the laterally extensive MTDs that overlie the erosional surface (labelled horizon V; e.g. Fig.8C-E), suggests that the former may derive from failures of the latter during major sediment-gravity flows. The *D* seismic facies interpreted as hemipelagic drape/muddy turbidites, where preserved, generally drape the erosional submarine channels and their infilling

26

(Fig. 7C-E, 8C-E). The detached, curved loops on the outer bends of the erosional channel associated with horizon V were interpreted as abandoned meander loops (Fig. 8A, B). The chaotic areas with overall low RMS amplitudes north and northeast of the study area (Fig. 8A, B) were interpreted as MTDs. The moderate RMS amplitudes associated with the MTDs to the northeast of the rounded, dark features (mobile shales; Fig. 7A), suggest the presence of sands within the MTDs that were trapped within local topography associated with the mobile shales (Fig. 8A, B). The short, east-west trending linear scars, adjacent to the mobile shales and the associated small, dark rounded features, were interpreted as fault scars and fluid escape features, respectively (Fig. 8A). The longer linear scars confined within the shorter (fault scars), characterised by coherent/slightly deformed internal architecture with moderate to high reflectivity on the seismic line (e.g. Fig. 2B, 5A) were interpreted as mobile shale-derived MTDs (see Chima *et al.,* 2019). The lateral confinement of these MTDs adjacent to the mobile shales (Figs. 8A, 9A), coupled with their somewhat coherent internal architecture and moderate to high RMS amplitudes, distinguish them from the regional MTDs (see Chima *et al.,* 2019). The elongated features, characterised by high RMS amplitude in the southern part of the study area (Fig. 9A), were interpreted as transient fan/lobe deposits (after Adeobga *et al.,* 2005). The winding features (CLSs) that cross the eastern transient fan/lobe suggest that sediment was bypassed on the eastern transient fan to a more distal setting beyond the limit of the 3D block we studied (Fig. 9A). The upward decrease in the thickness of slide/slump deposits from horizons R to W (Figs. 7C-E, 9C-E) suggests an overall decrease in the incisional ability of the sediment-gravity flows that sculpted the systems, or the gradual establishment of a local slope equilibrium profile in response to an overall decrease in shale tectonics. However, the upward decrease in the thickness of outer levees from the horizons R-W (Figs. 8C-E, 9C-E), suggests increased

confinement of sediment-gravity flows, or an overall decrease in the mud fraction of the former. The overall concave upward topography associated with erosional submarine channels in MSU 2, suggests that, prior to hemipelagic draping (e.g. Figs. 7C-E, 8C-E), they were underfilled compared to MSU 1, where erosional submarine channels were generally overfilled (e.g. Fig. 5B).

Based on the foregoing observations, three major changes occurred in the sedimentary records of the western Niger Delta intraslope basins over the last 5.5 Ma (see Figs. 3-10). These changes include (1) the lower part of MSU 1 at the transition between the late Messinian thick hemipelagic drape dated at 5.5 Ma (horizon M) to the overlying erosional surface (horizon A), characterised by relatively confined, erosional submarine channels, thin MTDs and channel levee deposits (e.g. Fig. 3A, B); (2) the upper part of MSU 1 at the transition between horizons G and I, dominated by thick, laterally extensive MTDs and partially confined, repetitive incisional submarine channels/erosional surfaces, with complex cut and architecture (e.g. Figs. 2A, 3A-C, 5A, B, 6A, B); (3) the transition between MSU 1 and MSU 2 (horizons P/Q), which marks the onset of repetitive, highly incisional, submarine channels/erosional surfaces that are infilled with aggrading/meandering channel levee complexes, thin MTDs and hemipelagic drapes (where preserved; see for e.g. Figs. 3A, B, 7C-E 8C-E).

4.4 Sequence stratigraphic interpretation of MSU 2

The preceding 3D geomorphological analysis reveals that MSU 1 and MSU 2 present different seismic facies and morphology (Figs. 3-10). Using the biostratigraphically constrained late Messinian (5.5 Ma), the modern seafloor (0 Ma), and taking the observed changes in the sedimentary architecture into account (Figs. 3-10), we suggest that the change at the transition

between MSU 1 and MSU 2 (P/Q) boundary could have occurred around 0.8-1.0 Ma during the Middle Pleistocene Transition (MPT) as described in the literature (0.8-0.9 Ma; Miller *et al.,* 2005; Lisiecki and Raymo; 2007; Fig. 10B, C). The eight seismic reflections identified in MSU 2 (horizons Q to X in Figs. 3-10), could represent eight fifth-order erosional surfaces (sequence boundaries). The hemipelagic drape, which marks the transition between MSU 1 and MSU 2 (horizon P), correlates with the moderate oxygen isotope (3.5%) and moderate sea-level variations (~12.5 m), before the more pronounced sea-level cycles with amplitudes reaching 100 m (Fig. 10B, C). This hemipelagic drape (horizon P), like horizon M at the lower part of MSU 1, was inferred to have been deposited during an overall high relative-sea level (see Chima *et al.,* 2019 and references therein). The assigned age (0.8-1.0 Ma) agrees with that attributed by Benjamin *et al.* (2015), who suggested that this conformable seismic surface belonged to the middle Pleistocene. The repetitive motifs consisting of vertically stacked erosional submarine channels, infilled with aggrading/meandering channel levee complexes (CLCs) and MTDs (slides/slumps?), and hemipelagic drapes (where preserved), e.g. (Figs. 3A, B; 7C-E; 8D, E), appear to record the regressive-transgressive cycles previously documented on the eastern Niger Delta continental shelf (e.g. Patoke and Bhattacharya, 2010; Jermannaud *et al.,* 2010; Riboulot *et al.,* 2011). Similar architectural elements have been documented in the deep-water setting, offshore the Rio Muni Basin (Equatorial Guinea), where the development of submarine canyons and their infilling turbidite systems were linked to a combination of allocyclic (relative sea level, tropical storms and tectonics), and autocyclic forcing, linked to submarine channel avulsions (see Jobe *et al.*, 2011). What is more, the submarine channels with similar architectural features described in this study (Figs. 3-10), have been recorded in the deep-water Bowser Basin,

Northern British Columbia (Canada), where slope gullies and their infilling turbidite systems were linked to relative sea-level changes and local slope failures (Ricketts and Evenchick, 1999).

From the foregoing observations, it is reasonable to infer that the erosional surfaces observed in MSU 2 (horizons Q-X), notably, the repetitive, highly incisional submarine channels associated with horizons R, S, V, W and X (e.g. Figs. 3A, B; 7C-E, 8C-E), could represent what we call 'the falling stage erosional surfaces' (FSESs; Fig. 12), equivalent to the basal surface of forced regression (BSFR) that are generally observed on the continental shelf (see Jermannaud *et al.,* 2010; Roby *et al.,* 2011; De Gasperi and Catuneanu, 2014; Catuneanu, 2020). Where deeply incised, the FSESs are locally overlain by the previously described basal MTDs or the bypass facies (e.g. Fig. 5B), which we interpreted as the falling stage systems tracts (see Posamentier and Kolla, 2003; De Gasperi and Catuneanu, 2014; Catuneanu, 2020). The infilling, aggrading/meandering channel levee complexes (CLCs) and MTDs (slide/slumps?) (Figs. 3A, B; 7C-E; 8C-E), were interpreted as lowstand to early transgressive systems tracts, while the hemipelagic drapes that generally cover the entire system (where preserved) (e.g. Figs. 3A, B; 7C-E; 8C-E), were interpreted as late transgressive to highstand systems tracts (see Posamentier and Kolla, 2003; De Gasperi and Catuneanu, 2014; Catuneanu, 2020). These architectural elements are rarely completely preserved either inside or outside the erosional submarine channels due to incessant mass wasting on the western Niger Delta slope (e.g. Figs. 2-10).

The estimated duration of the sequence in MSU 2 (see section 4.6 below), suggests that these architectural elements may have been controlled by glacio-eustatic sea-level oscillations over the last circa 0.8-1.0 Ma (see Miller *et al.,* 2005; Lisiecki and Raymo; 2007; Fig. 10B, C). The estimated age of the last erosional surface in MSU 2 (horizon X; Figs. 3A, 10B, C) was interpreted as the LGM, at around ~20 ka, as also suggested by Jobe *et al.,* (2015; 2016).

4.5 Sequence stratigraphic interpretation of MSU 1

Based on the above interpretation of MSU 2, MSU 1 could correspond to a deposition between 5.5 Ma and 0.8 Ma (horizons M-P), with the 11 erosional surfaces (labelled A to K), representing 11 fourth-order FSESs (sequence boundaries; Fig. 10B, C). Although, we included the hemipelagic drape (horizon M, dated at 5.5 Ma) in MSU 1 for calibration of the lower part of the MSU 1, the overlying erosional surface (labelled horizon A), which marks the onset of MTDs and channel levee deposits (Fig. 3B), was interpreted as the actual basal limit of MSU 1. The erosional surface associated with horizon A correlates with a high oxygen isotope value (> 4.5%), and one of the highest falls in the relative sea-level (> 25 m) during the early Pliocene (Fig. 10B, C). We suggest an age of 4.9 Ma for the 185 m deep erosional surface, reasoning that it could be correlated with the first major fall in sea level just after the late Miocene (5.5 Ma) high sea level (see Miller *et al.,* 2005; Lisiecki and Raymo, 2007; Raymo *et al.,* 2018; Fig. 10B, C). The 4.9 Ma we propose for this erosional surface (horizon A in Fig. 10B, C), disagrees with the late Miocene proposed by Benjamin *et al.* (2015), who lacked biostratigraphic control. The occurrence of the A horizon just above the hemipelagic drape dated at 5.5 Ma, its erosional character (Fig. 3A-C, 7C-E, 8C-E), and association with MTDs and CLSs, further support its nomination as a possible candidate for the fall in sea level in the early Pliocene around 4.9 Ma (see Miller *et al.,* 2005; Lisiecki and Raymo, 2007; Raymo *et al.,* 2018; Fig. 10B, C).

The transition at the upper part of MSU 1 (the G/I interface), is an ~120-m deep erosional surface (e.g. Fig. 4B), which tentatively correlates with a (> 30) m fall in the relative sea level and relatively high oxygen isotope (> 3.5%) (Fig. 10B, C). The erosional character of this surface coupled with its association with multiple CLSs (e.g. Fig. 4A, B), suggest that it could

have developed during a lowering of the relative sea level. The 176 m deep relief associated with horizon I (just above horizon G in Fig. 5B) and its complex cut and fill architecture, resemble the erosional submarine channels observed in MSU 2 (e.g. horizons R, V, W in Figs. 7, 8, 9A). The 176 m deep erosional submarine channel associated with horizon I and the overlying basal MTDs (bypass facies; e.g. Fig. 5B), could be interpreted as the falling stage erosional surface (FSES) and falling stage systems tracts, respectively (see Posamentier and Kolla, 2003; De Gasperi and Catuneanu, 2014; Catuneanu, 2020. Similarly, the infilling turbidite feeder channels/aggrading or meandering CLCs (e.g. Fig. 5B) could be interpreted as lowstand to early transgressive systems tracts, while the overlying hemipelagic drape could represent the late transgressive to highstand systems tracts (e.g. 5B, 6B).

The transition from CLS dominated intervals to repetitive, highly incisional submarine channels and mass-wasting dominated intervals is visible around horizons G and I (e.g. Figs. 3, 4, 5). This change in the sedimentary architecture could be associated with a fall in the relative sea level probably during the early Pleistocene, following the Northern Hemisphere Glaciation (NHG), which, in the literature, is documented to have occurred around 2.6 Ma (see Miller *et al.,* 2005; Lisiecki and Raymo, 2007, Gibbard *et al.,* 2010; Head and Gibbard, 2015a, b; Gibbard and Lewin, 2016; Raymo *et al.,* 2018; Fig. 10B, C). Hence, we propose erosional surfaces G and I as possible candidates for the early Pleistocene but favour the latter due to its repetitive, incisional and aggrading/meandering patterns that resemble those described in the deep-water western Niger Delta over the last circa 120 ka as controlled by glacio-eustatic sea-level oscillations and sediment supply (see Jobe *et al.,* 2015; 2016).

4.6 Sequence duration and sedimentation rates in MSU 1 and MSU 2

Sequence duration measures the ratio of the time interval for seismic unit development to the number of enclosed seismic surfaces (see Zhang *et al.,* 2019). Using the estimated ages above, the sequence duration for MSU 1 yields (5.5-0.8) Ma/13= ~0.4 Ma (~400 ka) and (0.8-0) Ma/8 = ~0.1 Ma (~100 ka) for MSU 2. Using an average velocity of 1253.2 m/s obtained from Well-1 (W1) (Fig. 1E), the estimated sedimentation rates in non-decompacted MSU 1 and 2 are132 m/Ma and 370 m/Ma, respectively.

5. Discussion

We discuss the Pliocene and Pleistocene stratigraphic evolution of the western Niger Delta intraslope basins over the last 5.5 Ma in relation to allocyclic (glacio-eustatic) sea-level and basin tectonic forcings, and propose a deep-water depositional model.

5.1 Allocyclic (glacio-eustatic) sea-level forcing

Allocyclic factors refer to controls that are unrelated to the depositional system; these include climate, eustasy, tectonics and sediment supply (Einsele *et al.,* 1991). Orbital parameters, such as obliquity and eccentricity forcings control global sea level, climate, drainage basin erosion, sediment supply, and more locally, environmental energy, and consequently influence the architecture of sedimentary units and their bounding surfaces (Zecchin*,* 2007; 2010; 2012; Catuneanu and Zecchin, 2013).

High subsidence rates (350 m/Ma) offset by high sedimentation rates (36.5 cm/ka) have been shown to facilitate the preservation of eccentricity sequences of 100 ka on the eastern Niger Delta continental shelf over the last circa 0.5 Ma (Riboulot *et al.,* 2012), in agreement with observations of the Mediterranean margin over the last circa 0.5 Ma, where subsidence rates as

high as 255 m/Ma, accompanied by high sedimentation rates, enabled preservation of 100 ka

eccentricity sequences, linked to glacio-eustatic sea-level oscillations during the Quaternary (see

Rabineau *et al.* 2006; Leroux *et al.,* 2014). Although we did not estimate subsidence rates over

the last circa 5.5 Ma, the overall increase in the sedimentation rates (x3) at the MPT (0.8-1.0

Ma), possibly accompanied by high subsidence rates (see Goudie, 2005), is inferred to have

facilitated the preservation of the 100 ka sequences we observed in MSU 2. This interpretation is

also in agreement with that of Gulick *et al.* (2012), who documented an overall increase in the

sedimentation rates at a source-to-sink-scale on the New Jersey margin (USA), linked to glacio-

eustatic changes in sea level over the last 0.7-1.2 Ma.

Although the 400 ka eccentricity sequences we propose for MSU 1 are recognized to

have strongly influenced sedimentation in ocean basins (e.g. Pälike *et al.,* 2006; Boulila *et al.,*

2011), eccentricity has rarely been described in the deep basin architecture. MSU 1 displays a

400 ka sequence duration and is characterised by the ubiquity of discontinuous seismic

reflections, the preponderance of regional MTDs and erosional surfaces, characterised by

complex cut and fill architecture in the upper part of the unit (Fig. 3A, B, 5A, B). These

architectural features resemble the fourth-order incised valleys/slope canyons on the Foz do

Amazonas continental shelf that were biostratigraphically constrained and, based on seismic

records, calibrated as 400 ka eccentricity sequences in the Pliocene (see Gorini *et al.,* 2014).

Based on the repetitive motifs of erosional surfaces, the infilling aggrading/meandering channel

levee complexes, hemipelagic draping (Figs. 3-10) and the sequence durations estimated in MSU

1 and MSU 2, our interpretation is that depositional sequences in the two units were organised in

400 ka and 100 ka sequences, respectively (Fig. 10B, C).

The Pliocene and the Pleistocene stratigraphy of the western Niger Delta intraslope basins, respectively characterised by mass-wasting and turbidite sequences, and by hemipelagic drapes and turbidite sequences (Figs. 3-10), is also comparable with the Pliocene and the Pleistocene stratigraphy of the Ulleung Basin, East Sea (Japan), which is characterised by, respectively, debris-flows and turbidite sequences, and hemipelagic drapes and turbidites sequences (see Yoo *et al.,* 2017). In the Ulleung Basin, the Pliocene stratigraphy is mainly linked to tectonic deformation, while the Pleistocene is linked to changes in the relative sea level (Yoo *et al.,* 2017). However, the Pliocene and Pleistocene stratigraphy described in the present study contrasts with that of the northern Gulf of Mexico (GOM), where tectonic subsidence is reported to have facilitated thick hemipelagic sedimentation/muddy turbidites and thin MTDs during the Pliocene compared to the Pleistocene, which is dominated by thick MTDs and thin hemipelagic sediments (Madof *et al.,* 2017; Wu *et al.,* 2020; Catuneanu, 2020). Madof *et al.* (2017) and Wu *et al.* (2020), showed that the stratigraphy of the northern Gulf of Mexico over last 3.7 Ma was mainly controlled by differential sedimentation and associated salt-related subsidence, while the overall increase in sedimentation rates over the Pleistocene was largely controlled by the capture of the Ohio and Missouri River by the Mississippi in the late Pleistocene (see also Prather *et al.,* 1998).

Pliocene and Pleistocene stratigraphy in the western Niger Delta intraslope basins was controlled by a combination of glacio-eustasy and shale tectonics (see discussion below). The observed increase in the sedimentation rates at the MPT (0.8-1.0 Ma), could be linked to (i) glacio-eustatic sea-level forcing linked to the Milankovitch cycles; (ii) regional climate forcing associated with the West African Monsoon, which has been shown to have interacted with drainage basins, erosion, and the supply of sediment to the Niger Delta since the Plio-Quaternary

35

(see Lézine et *al.* (2005; Weldeab *et al.,* 2011; Collins *et al.,* 2014; Govin *et al.,* 2014; Armitage *et al.,* 2015); (iii) a possible shift in sediment fluxes from the eastern to the western Niger Delta over the Pleistocene due either to delta lobe switching/regional climate evolution (see Jermanaud *et al.*, 2010; and references therein), or tectonic reorganisation of the catchment (e.g. Goudie, 2005). A recent study by Picot *et al.* (2019) in the adjacent Congo Basin demonstrated an overall architectural submarine channels avulsion that can be applied to most progradation/retrogradation patterns in response to climate forcing.

5.2 Basin tectonics

In terms of basin tectonics, control of the Pliocene and Pleistocene stratigraphy of the western Niger Delta intraslope basins, Chima *et al* (2019), showed that the main erosional submarine channel in the study area (labelled 1, 2, 3; Fig. 11A, B), has been active since the Pliocene, and was generally deflected to the southern part of the study area with east-west orientation during the early and late active periods of mobile shales (stages 1 and 3 in Fig. 11A, B), and northwards, with a northeast-southwest orientation during quiescent shale tectonics (stage 2 in Fig. 11A, B). In the present study, we investigated the entire submarine channel systems over the last 5.5 Ma, and provide a better understanding of the control of basin tectonics and deep-water depositional systems (Fig. 11A, B).

The progressive shift of erosional submarine channel levee systems from the NW to the SE in MSU 1 (stages 1a-c; Fig. 11A) could be linked to avulsion events in response to (i) shale tectonics or (ii) changes in sediment supply. Similarly, the absence of submarine channels in the northern part of the study area in MSU 2 (Fig. 11B) could be due to (i) up-dip channel avulsions in response to the movement of mobile shales (see also Clark and Cartwright, 2012; Jolly *et al.,*

36

2016) or (ii) shifting of the depositional axis further NW, away from the study area. The lateral

variation in the stratigraphic thickness of MSU 1 (5.5 to 0.8-1.0 Ma), compared to MSU 2 (0.8-

1.0 to 0 Ma), suggests that shale tectonics was more active in the Pliocene than in the Pleistocene

(e.g. Figs. 3B, 10B). The presence of mobile shales, mud volcanoes, pockmarks, BSR, fluid

escape features and mobile shale-derived MTDs (see for example, Figs. 1E; 3A, B, 5A, 8A-C,

9A), support local control by shale tectonics over slope depositional patterns (see Chima *et al.,*

2019). The local increase in the CLS gradient down-dip of the mobile shale in Fig. 11B, the

inversion of some normal faults during the Pleistocene (e.g. of the Z fault in Fig. 3B), and the

presence of mud volcanoes on the modern seafloor (Figs. 1E, 3A, B), further support movement

of mobile shale on the western Niger Delta slope during the Pleistocene (see also Chima *et al.,*

2019). These observations, therefore, call for caution concerning the widespread assumption that

mobile shales in the Niger Delta were buried during the late Pliocene (e.g. Cohen and McClay,

1996; Wiener *et al.,* 2010; Morley *et al.,* 2011).

5.3 Depositional model

Despite the dissimilar seismic facies association in MSU 1 and MSU 2 (e.g. Fig. 2B, C),

the overall sedimentary architecture observed in the two units (Figs. 3-10), suggests that

allogenic forcings at different scales and basin tectonics controlled the stratigraphic evolution of

the western Niger Delta intraslope basins over the last 5.5 Ma. Comparing our observations in

MSU 1 and MSU 2 (Figs. 2-10) with published depositional models (e.g. Posamentier and Kolla,

2003; De Gasperi and Catuneanu, 2014; Catuneanu, 2020), produced in a generalized facies

association (Fig. 12) and a 3-dimensional depositional model (Fig. 13A-E) which explain the

long-term stratigraphic evolution of the western Niger Delta slope over the last 5.5 Ma.

5.3.1 Falling stage

Falling is controlled solely by episodes of relative sea-level falls and is the key criterion for the definition of stratigraphic cyclicity in deep-water settings (Posamentier and Kolla, 2003; De Gasperi and Catuneanu, 2014; Catuneanu, 2020). The highly incisional erosional surfaces we observed in MSU 1 and MSU 2 (e.g. Figs. 3, 5, 7, 8, 9A), which we interpreted as the falling stage erosional surfaces (FSESs; Fig. 12), were inferred to have developed respectively during the fourth- and fifth-order falling stage sea-level, erosion and bypass processes on the slope (Fig. 13A). While the basal MTDs, which locally overlie the FSESs (e.g. Fig. 5B), could represent the falling stage system tracts (Fig. 13A), high-density grain/mud flows are inferred to have delivered sandy to muddy submarine fans to the basin floor (Catuneanu, 2020). The occurrence of basal MTDs at the bases of the erosional submarine channels associated with horizons A and I (e.g. Figs. 3B, 4B, 5B, 7C, 8C), suggest that sediment-gravity flows were rich in mud and were partly sequestered in erosional submarine channels on the slope on their way to the deep basin (Fig. 13A). Similar observations have been reported in the deep-water eastern Niger Delta, where MTDs were calibrated with core data and shown to be mud-rich (debris flows), linked to fourth-order relative sea-level fall (see Zhang *et al.,* 2019). The overall absence of MTDs at the bases of the erosional submarine channels in MSU 2, suggests that the former was eroded or not deposited in erosional submarine channels in this unit unlike in MSU 1 (compare Figs. 3A, B, 5B, 7C-E; 7C-E). Similarly, the paucity of MTDs in MSU 2 (e.g. Figs. 3A, B; 10A-C), could be related to overall changes in the sediment supply/calibre, the flow dynamics, or the relatively quiescent shale tectonics over the Pleistocene.

5.3.2 Lowstand

The turbidite feeder channels/aggrading or meandering channel levee complexes (CLCs) are the most dominant seismic facies described in the two FSESs (Figs. 3-10). In the complex infilling of erosional submarine channels, the ubiquity of successive erosions and mass-flow deposits render interpretation more complex (e.g. Figs. 3B; 7C-E, 8C-E). The turbidite feeder channels/aggrading or meandering channel levee complexes (CLCs) and/or MTDs (slides/slumps) which generally infill the erosional submarine channels in MSU 1 (e.g. Figs. 4B, 5B, 6B, 7C, 10B) and MSU 2 (e.g. Figs. 3A, B, 7C-E, 8C-E), were inferred to have been developed during the lowstand/early transgression (see Catuneanu, 2020; Fig. 12B, C). Similarly, the regional MTDs previously interpreted to have been sourced from the upper slope/shelf-margin (see Chima *et al.*, 2019; e.g. Figs. 3A, B; 5B 3C; 9B; 10A, B), were inferred here to be lowstand/early transgressive deposits (Fig. 12B, C). The high amplitude reflectivity (HARS) of the turbidite feeder channels/aggrading or meandering channel levee complexes character, suggests that they were deposited from sand-rich sediment-gravity flows (see also Chapin *et al.,* 2002; Deptuck *et al.,* 2003; Heiniö and Davies, 2007; Jobe *et al.,* 2011; 2015). Although slope overstepping by normal and reverse faulting are known to trigger mass failures on the slope (e.g. Ricketts and Evenchick, 1999; Fatoke and Bhattacharya, 2010; Chima *et al.*, 2019), the overall association of the regional MTDs with erosional events that correlate with relative sea-level lowering (e.g. horizon A in Fig. 3A, B; 10B, C), supports the interpretation of the former as lowstand deposits (see Posamentier and Kolla, 2003; De Gasperi and Catuneanu, 2014; Catuneanu, 2020). Low density turbidity currents and fine grain flows have been described as the main processes during the lowstand/early transgression (Catuneanu, 2020). Slope depositional

patterns during the lowstand may have been locally influenced by the movement of mobile shales and associated fluid flows (see Riboulot *et al.,* 2012; Figs. 1D; 3A, B; 8A, 9A, 13C).

5.3.4 Transgression to Highstand

The thick hemipelagic sediments that generally drape the entire system, where preserved (e.g. Figs. 3B, 7C-E, 8C-E), were inferred to have been deposited during the late transgressions/highstands, when the deep-water settings were starved of clastic sediment (see Posamentier and Kolla, 2003; De Gasperi and Catuneanu, 2014; Catuneanu, 2020; Fig. 13D). The conformable nature of the hemipelagic drape (e.g. Figs. 3B, 7C-E, 8C-E), their mud-rich nature inferred from moderate gamma-ray log patterns (e.g. Fig. 13D) and their association with *Discoaster qinqueramus* as recorded in Well 3 (W3) (Fig. 13D), support their interpretation as transgressive/highstand deposits (see also Clima *et al.,* 2019). Hemipelagic sedimentation is inferred to have punctuated deep-water deposition by shutting down sediment-gravity flows (see Burgess *et al.,* 2008)

The foregoing processes were inferred to have occurred thirteen times in MSU 1 and eight times in MSU 2 (e.g. Fig. 10B, C). A simplified schematic diagram illustrating the long-term (4/5th-order sea-level controlled) incision, infilling and hemipelagic draping of submarine channels on the western Niger Delta slope is shown in Fig. 13E. Although the proposed model mainly hinges on long-term changes in relative sea level, our observations suggest that shale tectonics locally influenced depositional patterns on the western Niger Delta intraslope basins over the last 5.5 Ma.

6 Conclusions

Detailed seismic stratigraphy and 3D geomorphological analysis of high-resolution 3D seismic data over the Pliocene and Pleistocene stratigraphic record of the western Niger Delta intraslope basins, showed that:

1. Glacio-eustatic sea-level changes since the last 5.5 Ma are recorded at regional scale in the intraslope basins of the western Niger Delta.

2. The depositional sequence in the intraslope basins of the western Niger Delta is generally defined by the falling stage erosional surface (FSES) at its base and top (sequence boundary), and is characterised by (i) basal MTDs/bypass facies (where preserved), (ii) turbidite feeder channels/aggrading or meandering channel levee complexes and/or MTDs (slides/slumps) and (iii) hemipelagic drape that successively represent the falling stage, lowstand to early transgressive, and late transgressive to highstand systems tracts.

3. The Pliocene and Pleistocene stratigraphy of the western Niger Delta intraslope basins was controlled by allocyclic forcing linked to glacio-eustatic sea-level oscillations and basin tectonics associated with mobile shales, the latter being most active during the Pliocene and the middle Pleistocene.

4. The overall higher sedimentation rate over the MPT (0.8-1.0 Ma to present) possibly accompanied by subsidence was inferred to have facilitated the preservation of the 100 ka sequences in MSU 2 compared to MSU 1 (5.5 to 0.8-1.0 Ma), where a slower sedimentation rate was inferred to have favoured the preservation of the 400 ka sequences.

5. This seismic stratigraphic study demonstrates for the first time sequence cyclicity associated with orbital (Milankovitch) forcing in the deep-water western Niger Delta and if calibrated

41

with biostratigraphic data in future studies, could serve as a useful analogue for further studies in the Gulf of Guinea, the equatorial Atlantic and other margins fed by large deltas.

An ongoing study is investigating the control of delta top extensional tectonics over sediment sequestration/bypass on the shelf and its implication for gravity tectonics in the western Niger Delta.

Conflict of interest

References

Adeogba, A.A., McHargue, T.R., and Graham, S.A. 2005, Transient fan architecture and depositional controls from near-surface 3D seismic data, Niger Delta continental slope. AAPG Bulletin 89, 627–643.

Armitage, S.J., Bristow, C.S., Drake, N.A, 2015, West African monsoon dynamics inferred from abrupt fluctuations of Lake Mega-Chad. PNAS 112 (28), 8543-8548.

Backman, J., Raffi, I., Rio, D., Fornaciari, E., Pälike, H., 2012, Biozonation and biochronology of Miocene through Pleistocene calcareous nannofossils from low and middle latitudes. Newsl. Stratigr. 45, 221–244. https://doi.org/10.1127/0078-0421/2012/0022.

Bakare, O., Hurley, N., and McHargue, T., 2007, Effect of Growing Structures on Stratigraphic Evolution, Channel Architecture, and Submarine Fan Distribution, Niger Delta, West Africa. AAPG Conference Proceedings, California.

Bassinot, F.C., Labeyrie, L.D., Vincent, E., Quidelleur, X., Shackleton, N.J., and Lancelot, Y., 1994, The astronomical theory of climate and the age of the Brunhes-Matuyama magnetic reversal. Earth and Planetary Science Letters 126, 91–108

Bellingham, P., Connors, C., Haworth, R., Barbara, R., Danforth, Al, 2014. The deep-water Niger delta: an underexplored world class petroleum province. Petrol. Geosci. Mag. 11, 1–9.

Benjamin, U. K., House, M., and Hodgetts, D., 2015, Canyon-confined pockmarks on the western Niger Delta slope. Journal of African earth Sciences 107, 15-27.

Bilotti, F. D., Shaw, J. H., Cupich, R.M., and Lakings, R.M., 2005, Detachment fold, Niger Delta, in J. H. Shaw, C. Connors, and J. Suppe, eds., Seismic interpretation of contractional fault related folds: AAPG Studies in Geology 53, 103– 104.

Boulila, S., Galbrun, B., Miller, K. G., Pekar, S. F., Browning, V. B., Lasker, J., Wright, J. D., 2011., On the origin of Cenozoic and Mesozoic "third-order" eustatic sequences. Earth-Sciences Reviews (3-4), 94-112.

Burbank, D.W., 1992, Causes of recent Himalayan uplift deduced from deposited patterns in the Ganges basin. Nature, 357, 680–683.

Burgees, P. M., Steel, R. J. and Granjeon, D., 2008. Stratigraphic forward modeling of basin-

margin clinoform systems: implications for controls on topset and shelf width and timing of formation of shelf-edge deltas. SEPM 90, 35-45.

Catuneanu, O., 2006, Principles of sequence stratigraphy. Elsevier, Amsterdam, 386.

Catuneanu, O., Galloway, W. E., Kendall, C. G. St. C., Miall, A. D., Posamentier, H. W., Strasser,
      S., and Tucker, M. E., 2011, Sequence stratigraphy: Methodology and Nomenclature.
      Newsletter on Stratigraphy, 44 (3), 173-245.

De Gasperi, A., Catuneanu, O., 2014. Sequence stratigraphy of the Eocene turbidite reservoirs
      in Albacora field, Campos Basin, offshore Brazil. Am. Assoc. Petrol. Geol. Bull. 98 (2),
      279-313.

Catuneanu, O., 2020, Seqquence stratigraphy of deepwater systems. Marine and Petroleum
      Geology, 114 (104238). DOI: https://doi.org/10.1016/j.marpetgeo.2020.104238

Chapin, M., Swinburn, P., van der Weiden, R., Skaloud, D., Adesanya, S., Stevens, D., Varley, C.,
      Wilkie, J., Brentjens, E., and Blaauw, M., 2002, Integrated seismic and subsurface
      characterization of Bonga Field, offshore Nigeria. The Leading Edge 21, 1125-113.

Chima, K. I., Do Couto D., Leroux, E., Gardin S., Hoggmasacall, N., Rabineau, M., Granjean, D.,
      and Gorini, C., 2019, Seismic stratigraphy and depositional architecture of Neogene
      intraslope basins, offshore western Niger Delta. Marine and Petroleum Geology 109,
      449-468. doi: 10.1016/j.marpetgeo 2019.06.030

Chopra, S., and Marfurt, K.J., 2007, Seismic attributes for prospect identification and reservoir
      characterization. Tulsa, Oklahoma, 457.

Clark, I. R. and Cartwright, J. A., 2012, Interactions between coeval sedimentations and
      deformation from the Niger Delta deep-water fold belt. SEPM 3, 243-267.

Clift, P.D., 2010, Enhanced global continental erosion and exhumation driven by Oligo-Miocene
      climate change. Geophys. Res. Lett., 37, L09402.

Cohen, H.A., and McClay, K., 1996, Sedimentation and shale tectonics of the northwestern
      Niger Delta front. Marine and Petroleum Geology 13, 313-328.

Collins, J.A., Schefuß, E., Govin, A., Mulitza, S., Tiedemann, R., 2014, Insolation and glacial-
      interglacial control on southwestern African Hydroclimate over the last 140,000 years.
      Earth and Planetary Science Letters 398, 1-10.

Connors, C. D., Denson, D. B., Kristiansen, G. and Angstadt, D. M., 1998, Compressive
      anticlines of the mid-outer slope, central Niger Delta (abs.) AAPG Bulletin, 82, 1903.

Corredor, F., Shaw, J.H., and Bilotti, F., 2005, Structural styles in the deep-water fold and

thrust belts of the Niger Delta. AAPG Bulletin 89, 753780. https://doi.org/10.1306/02170504074

Crutchley, G.J., Klaeschen, D., Planert, L., Bialas, J., Berndt, C., Papenberg, C., Hensen, C., Hornbach, M., Krastel, S., Brueckmann, W., 2014, The impact of fluid advection on gas stability: investigation at sites on methane seepage, offshore Costa Rica. Earth and Planetry Science Letters 401, 95-109.

Damuth, J. E., 1994, Neogene gravity tectonics and depositional processes on the deep Niger Delta continental margin: Marine and Petroleum Geology, 11, 320–346.

Davies, R. J., 2003, Kilometer-scale fluidization structures formed during early burial of a deep-water slope channel on the Niger Delta. GSA 31 (11) 949-952.

Deptuck, M.E., Steffens, G.S., Barton, M., Pirmez, C., 2003. Architecture and evolution of upper fan channel-belts on the Niger Delta slope and in the Arabian Sea. Marine and Petroleum Geology 20, 649-676.

Deptuck, M.E., Sylvester, Z., O'Byrne, C., 2012, Pleistocene seascape evolution above a "simple"
stepped slope-western Niger Delta, in: Prather, B.E., Deptuck, M.E., Mohrig, D., Van Hoorn, B., Wynn, R.B. (Eds.), Application of the Principles of Seismic Geomorphology to Continental-Slope and Base-of-Slope Systems: Case Studies from Seafloor and Near-Seafloor Analogues, pp. 199-222.

Doust, H., and Omatsola, E., 1990, Niger Delta, in J. D. Edwards and P. A. Santogrossi, (Eds.); Divergent passive margin basins AAPG Bulletin 48, 239-248.

Einsele, G., Ricken, W., Seilacher, A., 1991, Cycles and Events in Stratigraphy. Springer-Verlag, Berlin, 955.

Eldefield, H., Ferretti, P., Greaves, M., Crownhurst, S. J., McCave, I. N., Hodell, D. A., Piotrowski, A. M., 2012, Stable Oxygen isotope record and Mg/Ca ratios at the Mid-Pleistocene Climate Transition, ODP Site 181-1123. Pangea. Doi: doi.org/10.1594/PANGAEA.786205.

Elliott, T.,1975, the sedimentary history of a delta lobe from a Yoredale (Carboniferous) cyclothem. Yorkshire Geological Society, Proceedings 40, 505-536.

Evamy, B.D., Haremboure, J., Kammerling, R., Knaap, W.A., Molloy, F.A., and Rowlands, P.H., 1978, Hydrocarbon habitat of Tertiary Niger Delta. AAPG Bulletin 62, 1-39.

Fatoke, O.A., Bhattacharya, J.P., 2010, Controls on Depositional Architecture and Sequence Stratigraphy of the Pliocene-Pleistocene Strata of Eastern Niger Delta, Nigeria. AAPG, Abstract, Denver.

Galloway, W. E., 2001, Cenozoic evolution of sediment accumulation in deltaic and shore-zone

depositional systems, northern Gulf of Mexico Basin: Marine and Petroleum Geology, 18, 1031-1040.

Gibbard, P. L., Head, M. J, Walker, J. C., 2010, Formal ratification of the Quaternary System/Period and the Pleistocene Series/Epoch with a base at 2.58 Ma. Journal of Quaternary Science 25 (2), 96-102.

Gibbard, P. L., Head, M.J., and Walker, M.J., 2014, Subcomission on stratigraphy Formal ratification of the Quaternary System/Period and Pleistocene Series/Epoch with a base at 2.5 Ma. Quaternary Science 245, 96-102.

Gibbard, P.L., Lewin, J., 2016, Partitioning the Quaternary. Quaternary Science Reviews 151, 127-139.

Gorini, C., Haq, B.U., dos Reis, A.T., Silva, C.G., Cruz, A.M, Soares, E., and Grangeon, D., 2014, Late Neogene sequence stratigraphic evolution of the Foz do Amazonas Basin, Brazil. Terra Nova, 26, (3), 179-185. https://doi.org/10.1111/ter.12083

Goudie, A. S., 2005, the drainage of Africa since the Cretaceous. Gemorphology (3-4), 437-456.

Govin, A., Varma, V., Prange, M., 2014, Astronomically forced variations in western African rainfall (21°N-20°S) during the Last Interglacial period. Geophysical research Letters 41, 2117-2125. doi:10.1002/2013GL058999.

Gulick, S.P., Jaeger, J.M., Mix, A.C., Asahi, N., Bahlburg, H., Belanger, C.L., Berbel, G.B., Childress, L., Cowan, E., Drab, L., Forwick, M., 2015, Mid-Pleistocene climate transition drives net mass loss from rapidly uplifting St. Elias Mountains, Alaska. Proc.Natl. Acad. Sci. Unit. States Am. 112, 15042-15047.

Hansen, L., Janocko, M., Kane, I., Kneller, B., 2017. Submarine channel evolution, terrace development, and preservation of intra-channel thin-bedded turbidites: Mahin and Avon channels, offshore Nigeria. Mar. Geol. 383, 146–167. https://doi.org/10.1016/j.margeo.2016.11.011

Haq, B.U., Hardenbol, J., Vail, P.R., 1987. Chronology of fluctuating sea levels since the triassic. Science 235, 1156–1167.

Head, M.J., Gibbard, P.L., 2015a, Early-Middle Pleistocene transitions: linking terrestrial and marine realms. Quat. Int. 389, 7-46. http://dx.doi.org/10.1016/j.quaint.2015.09.042

Head, M.J., Gibbard, P.L., 2015b, Formal subdivision of the Quaternary System/Period: past, present, and future. Quat. Int. 383, 1-32.

Heiniö, P., and Davies, R. J. 2007, Knickpoint migration in submarine channels in response to fold growth, western Niger Delta. Marine and Petroleum Geology 24, 434-449. doi.org/10.1016/j.marpetgeo.2006.09.002

Imbrie, J., Berger, A., Boyle, E.A., Clemens, S.C., Duffy, A., Howard, W.R., Kukla, G.,

Kutzbach, J.E., Martinson, D.G., McIntyre, A., Mix, A.C., Molfino, B., Morley, J.J., Peterson, L.C., Pisias, N.G., Prell, W.L., Raymo, M.E., Shackleton, N.J., and Toggweiler, J.R.,1993, On the structure and origin of major glaciation cycles 2. The 100,000-year cycle. Paleoceanography 8, 699-735.

Jermannaud, P., Rouby, D., Robin, C., Nalpas, T., Guillocheau, F., and Raillard, S., 2010, Plio-Pleistocene sequence stratigraphic architecture of the eastern Niger Delta: A record of eustasy and aridification of Africa. Marine and Petroleum Geology 27, 810-821.

Jervey, M.T.,1988, Quantitative geological modelling of siliclastic rock sequences and their seismic expressions. In: Wilgus, C.K., Hastings, B.S., St Kendall, C.G., Ross, C.A., Van Wagoner, J.C. (Eds.), Sea-level Changes: An Integrated Approach. SEPM Special Publication, Tulsa, 47-69.

Jobe, Z.R., Lowe, D. R., Uchytil, S.J., 2011, Two fundamentally different types of submarine canyons along the continental margin of Equatorial Guinea. Marine and Petroleum Geology 28, 843-860.

Jobe, Z.R., Sylvester, Z., Parker, A.O., Howes, N., Slowey, N., Pirmez, and C., 2015, Rapid adjustment of submarine channel architecture to changes in sediment supply. Journal of Sedimentary Research 85, 729-753.

Jobe, Z.R., Sylvester, Z., Howes, N., Pirmez, C., Parker, A., Cantelli, A., Smith, R., Wolinsky, M.A., O'Byrne, C., and Slowey, N., 2016, High resolution, millennial-scale patterns of bed compensation on a sand-rich intraslope submarine fan, western Niger Delta slope. GSA Bulletin 129, 23-37.

Jolly, B.A., Lonergan, L., Whittaker, A.C., 2016. Growth history of fault-related folds and interaction with seabed channels in the toe-thrust region of the deep-water Niger Delta. Mar. Pet. Geol. 70, 58–76.

Lafosse, M, Gorini, C, Le Roy, P., Alonso, B., D'Acremonta, E., Ercilla, G., Rabineau, M., Vázquez, J. T., Rabaute, R., Ammar, A., 2018, Late Pleistocene-Holocene history of a tectonically active segment of the continental margin (Nekor basin, Western Mediterranean, Morocco. Marine and Petroleum Geology 97, 370-389.

Leroux, E., Rabineau, M., Aslanian, D., Gorini, C., Droz, L. and Granjeon, D., 2014, Stratigraphic simulation on the shelf of the Gulf of Lions: testing subsidence rates and sea-level curves during Pliocene and Quaternary. Terra Nova, 26, 230-238.

Leroy, S.A.G., Wrenn, J.H., Suc, J.P., 1999, Global setting to comparative charts of regional events. In: Wrenn, J.H., Suc, J.P., Leroy, S.A.G. (Eds.), The Pliocene: Time of Change. American Association of Stratigraphic Palynologist Foundation, 1-12.

Lisiecki, L.E., and Raymo, M.E., 2005, A Pliocene-Pleistocene stack of 57 globally distributed benthic δ^{18}O records. Paleoceanography 20, PA1003. doi:10.1029/2004PA001071.

Lisiecki, L.E., and Raymo, M.E., 2007, Plio-Pleistocene climate evolution: trends and transitions
in glacial cycle dynamics. Quaternary Science Reviews 26, 46-69.

Lézine, A-M., Bassinot, F., Peterschmitt, J-Y., 2014, orbitally-induced changes of the Atlantic and
Indian monsoons over the past 20,000 years: New insights based on the comparison of continental and marine records

Madof, A.S., Christie-Blick, N., Anders, M.H., Febo, L.A., 2017, Unreciprocated sedimentation along a mud-dominated continental margin, Gulf of Mexico, U.S.A.: Implications for sequence stratigraphy in muddy settings devoid of depositional sequences. Marine and Petroleum Geology 80, 492-516.

Miall, A.D., 2010, The Geology of Stratigraphic Sequences, second ed. Springer-Verlag, Berlin, 522.

Miller, K.G., Kominz, M.A., Browning, J.V., Wright, J.D., Mountain, G.S., Katz, M.E., Sugarman, P.J., Cramer, B.S., Christie-Blick, N., and Pekar, S.F., 2005, The Phanerozoic Record of Global Sea Level Change. Science Magazine 310, 1293-1298.

Mitchum, R.M., and Vail, P.R., 1977, Seismic Stratigraphy and Global Changes of Sea Level, Part 7: Seismic Stratigraphic Interpretation Procedure: Seismic Stratigraphy: Applications to Hydrocarbon Exploration. AAPG Memoir 26, 135-143.

Morgan, R., 2004, Structural controls on the positioning of submarine channels on the lower slopes of the Niger Delta, in: Davies, R.J., Cartwright, J., Stewart, S.A., Underhill, J.R., Lappin, M. (Eds.), 3D Seismic Technology: Application to the Exploration of Sedimentary Basins. Geological Society of London Memoir 29, 45-51

Molnar, P., 2004, Late Cenozoic increase in accumulation rates of terrestrial sediment: how Might
Climate Change Have Affected Erosion Rates? Annu. Rev. Earth Planet. Sci., 32, 67-89.

Morley, C. K., King, R., Hillis, R., Tingay, M., Backe, G., 2011, Deep-water fold and thrust belt classification, tectonics, structure and hydrocarbon prospectivity. Earth Sciences Reviews 104, 41-91.

Picot M., Marsset T., Droz L., Dennielou B., Baudin F., Hermoso M., De Rafelis M., Sionneau T.,
Cremer M., Laurent D., Bez M., 2019, Monsoon control on channel avulsions in the Late Quaternary Congo Fan. Quaternary Science Reviews, 204, 149-171.

Pälike, H., Frazier, J., Zachos, J.C., 2006. Extended orbitally forced palaeoclimatic records from the equatorial Atlantic Ceara Rise. Quaternary Science Reviews 25, 3138–3149.

Posamentier, H.W., Jervey, M.T., and Vail, P.R., 1988, Eustatic controls on clastic deposition
   I. Conceptual framework. In: Wilgus, C.K., Hastings, B.S., Kendall, C.G.S.C.,
   Posamentier, H.W., Ross, C.A., Van Wagoner, J.C. (Eds.), Sea-Level Changes-an
   Integrated Approach. SEPM Special Publication 42, 102-124.

Posamentier, H.W., and Kolla, V., 2003, Seismic geomorphology and stratigraphy of depositional
   elements in deep-water settings. Journal of sedimentary research 73, 367–388.

Prather, B.E., Booth, J.R., Steffens, G.S., Craig, P.A., 1998, Classification, Lithologic Calibration
   and Stratigraphic Succession of Seismic Facies of Intraslope Basins, Deep- Water Gulf of
   Mexico. AAPG Bulletin 82 (5A), 701-728.

Prather, B.E., 2003, Controls on reservoir distribution, architecture and stratigraphic trapping in
   slope settings. Mar. Petrol. 20, 529–545

Prather, B.E., Pirmez, C., Sylvester, Z., and Prather, D. S., 2012 Stratigraphic Response to
   Evolving Geomorphology in a Submarine Apron Perched on the Upper Niger Delta
   Slope. SEPM 99, 145-161.

Pulham, A.J., 1989, Controls on internal structure and architecture of sandstone bodies within
   Upper Carboniferous fluvial-dominated deltas, County Clare, western Ireland. In:
   Whateley, M.K.G., Pickering, K.T. (Eds), Deltas: Sites and Traps for Fossil Flues.
   Geological Society, Special Publication, 41, 79-203.

Rabineau, M., Berné, S., Olivet, J-L., Aslanian, D., Joseph, P., and Guillocheau, F., 2006,
   Paleosea levels reconsidered from direct observation of paleo-shoreline position during
   Glacial Maxima (for the last 500 000 yr). Earth and Planetary Science Letters, 252
   (1-2), 119-137 DOI: 10.1016/j.epsl.2006.09.033

Rabineau, M., Leroux, E., Aslanian, D., Bache, F., Gorini, C., Moulin, M., Molliex, S., Droz,
   L., Dos Reis, T., Rabineau, J-L., Olivet, J-L., 2014. Quantifying subsidence and Isostasy
   using paleobathymetric markers : example from the Gulf of Lion, EPSL, vol. 388, p.
   353- 366.

Raymo, M. E., Kozdon, R., Evans, D., Lorraine, E., Lisiecki, L., Ford, H. L., 2018, The accuracy
   of mid-Pliocene δ^{18}O based ice volume and sea level reconstructions. Earth Science
   Reviews 177, 291-302.

Riboulot, V., Cattaneo, A., Lanfumey, V., Voisset, M., Cauquil, E., 2011, Morphological
   Signature of Fluid Flow Seepage in the Eastern Niger Submarine Delta (ENSD).
   Offshore Technology Conference.

Riboulot, V., Cattaneo, A., Berné, S., Schneider, R.R., Voisset, M., Imbert, P., Grimaud, S.,
   2012, Geometry and chronology of late Quaternary depositional sequences in the Eastern
   Niger Submarine Delta. Marine Geology, 319-322, 1-20.

Ricketts, B. D., Evenchick, C. D., 1999, Shelfbreak Gullies; Products of sea-level lowstands and

sediment failure: Examples from Bowser Basin, Northern British Columbia. SEPM 69 (6), 1232-1240.

Ridente, D., Trincardi, F., Piva, A., Asioli, A., Cattaneo, A., 2008, Sedimentary response to\ climate and sea level change during the past ~400 kyr from borehole PRAD1-2 (Adriatic Margin). Geochemistry, Geophysics, and Geosystems. 20 doi: http://dx.doi.org/10.1029/2007GC0017839/9Q09R04,

Rouby, D., Nalpas, T., Jermannaud, P., Robin, C., Guillocheau, F., and Raillard, S., 2011, Gravity driven deformation controlled by the migration of the delta front: The Plio-Pleistocene of the Eastern Niger Delta. Tectonophysics 513, 54-67. https://doi.org/10.1130/GEOSO1426.1

Ruddiman, W.F., Raymo, M.E., Martinson, D.G., Clement, B.M., and Backman, J., 1989, Pleistocene evolution: northern hemisphere ice sheets and North Atlantic Ocean. Paleoceanography 4, 353-412.

Shackleton, N.J., 2000, The 100,000-year Ice-Age cycle identified and found to lag temperature, carbon dioxide, and orbital eccentricity. Science 289

Taner, M.T., Schuelke, J.S., O'Doherty, R., and Baysal, E.,1994, Seismic attributes revisited. In: SEG technical program expanded abstracts 1994. https://doi.org/10.1190/1.1822709. Thornton, S.E., 1984. Hemipelagites and Associated Facies of Slopes and Slope Basins. In: Geological Society of London, Special Publications, 15, 377-394.

Tuttle, W.L.M, Brownfield, E.M., Charpentier, R.R., 1999, The Niger Delta Petroleum System Chapter A: Tertiary Niger Delta (Akata-Agbada) Petroleum System, Niger Delta Province, Nigeria, Cameroon and Equatorial Guinea, Africa. USGS, Open File Report. 99-50-H, 4-44.

Weldeab, S., Frank, M., Stichel, T., Haley, B., Sangen, M., 2011, Spatio-temporal evolution of the West African monsoon during the last deglaciation. Geophysical Research Letters, 38, L13703. doi:10.1029/2011gl047805.

Wiener, R.W., Mann, M. G., Angelich, M. T., and Molyneux, J. B., 2010, Mobile shale in the Niger Delta: Characteristics, structure, and evolution. AAPG, 93, 145-161.

Wu, N.N., Jackson, C. A-L., Johnson, H. D., Hodgson, D. M., Nugraha, H. D., 2020, Mass-transport complexes (MTCs) document subsidence patterns in 1 a northern Gulf of Mexico salt minibasin. Basin Research, 1-28. DOI: 10.1111/bre.12429

Yoo, D-G., Kim, K-Y., Kang, N-K., Yi, B-Y., Cho, M-H., 2017, Plio-Quaternary seismic stratigraphy and depositional history of the Ulleung Basin, East Sea: Association with debris-flow activity. Quaternary International, 459, 69-88

Zecchin, M. 2007, The architectural variability of small-scale cycles in shelf and ramp clastic

systems: the controlling factors. Earth-Sci. Rev., 84, 21-55.

Zecchin, M., Caffau, M., Tosi, L., Civile, D., Brancolini, G., Rizzetto, F., and Roda, C., 2010, The impact of Late Quaternary glacio-eustasy and tectonics on sequence development: evidence from uplifting and subsiding settings in Italy. Terra Nova 22, 324-329. doi: 10.1111/j.1365-3121.2010.00953.

Zecchin, M., Catuneanu, O. 2012, High-resolution sequence stratigraphy of clastic shelves I: units and bounding surfaces. Marine and Petroleum Geology 39, 1-25.

Zhang, J., Wu, S., Hu, G., Fan, T-E, Yu, B., Lin, P., Jiang, S., 2019, Sea-level control on the submarine fan architecture in a deep-water sequence of the Niger Delta Basin. Marine and Petroleum Geology 94, 179-197.
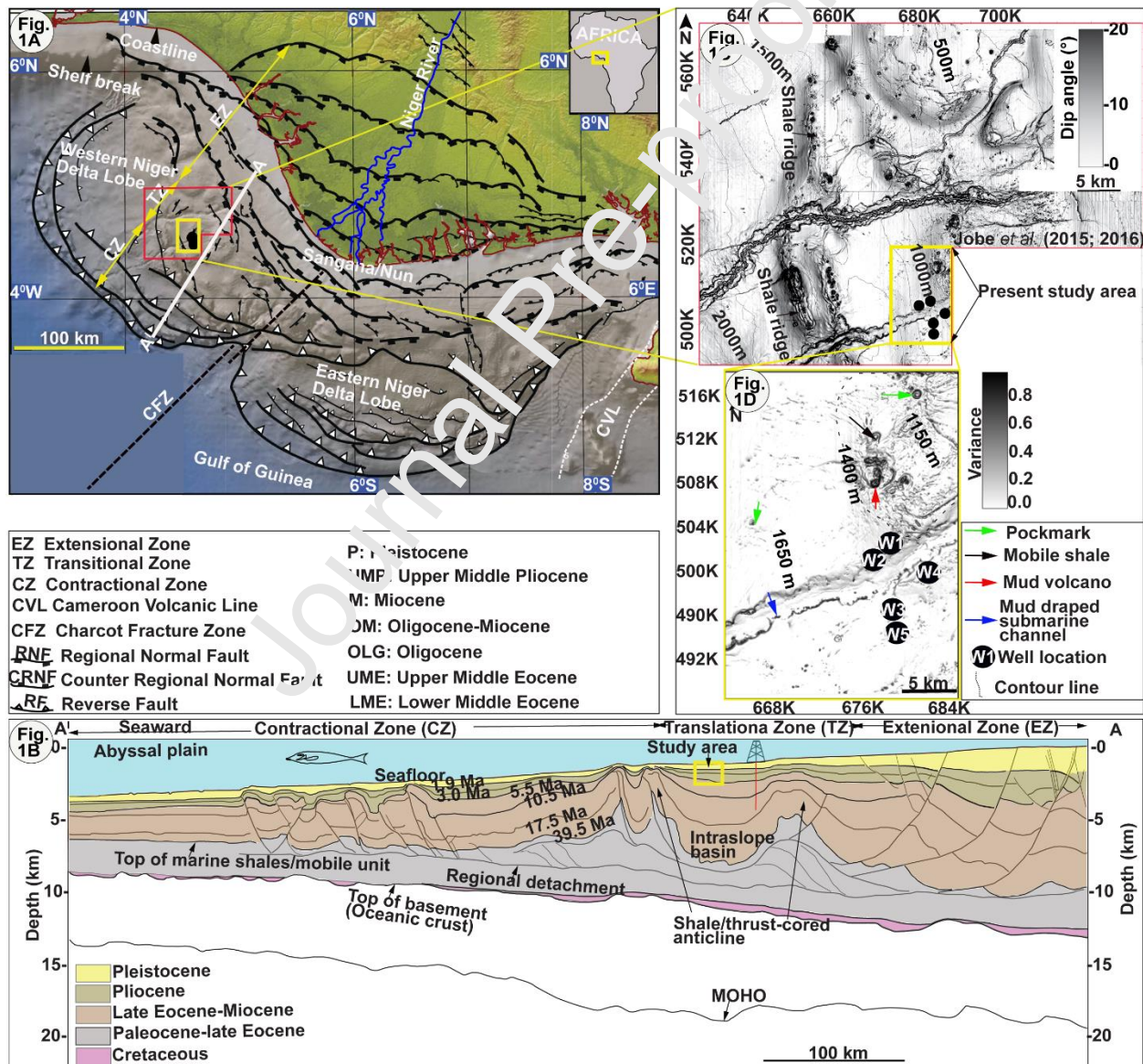
Fig. 1. Location of the study area. A: superimposed relief and bathymetric map showing the extensional zone (EZ), translational zone (TZ) and contractional zone (CZ) of the Niger Delta (adapted from Rouby et $al.,$ 2011). B: Seismic line drawing (AA^I) showing the styles of the structure (adapted from Bellingham et $al.,$ 2014). C: Dip in the seafloor showing the physiographic features of the translational zone (from Jobe et $al.,$ 2016). D: Depth structure map of the modern seafloor showing the presence of fluid flow features associated with mobile shales, mud volcanoes, pockmarks, and a mud-draped submarine channel in the study area (from Chima et $al.,$ 2019). Black circles in panels A, C (labelled W1-W5) in panel D indicate the locations of the wells.

	Seismic facies description	Seismic architecture	Line drawing	Pie map view	Interpretation
2a1	Chaotic, discontinuous, low-amplitude seismic facies				MTD (slides/slumps?)
2a2	Chaotic discontinuous to moderately continuous seismic facies				Turbidite feeder ch./ Aggrading or meandering channel levee complexes
2a3	Coherent/slightly inclined, moderate to high-amplitude seismic facies				Slide blocks/slump deposits
2a4	Parallel continuous to slightly convergent, high-amplitude seismic facies				Distributary channels/ lobe deposits
2a5	Convergent thinning, moderate to high-amplitude seismic facies				Channel levee /overbank deposits
2a6	Transparent, continuous draping seismic facies				Hemipelagic drape
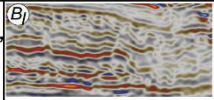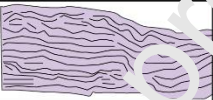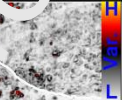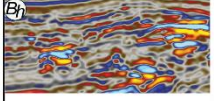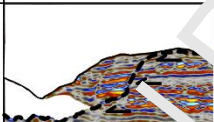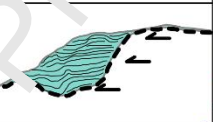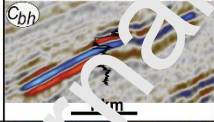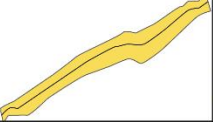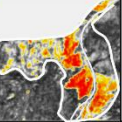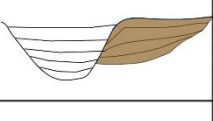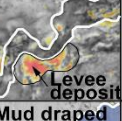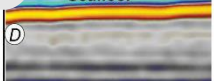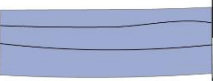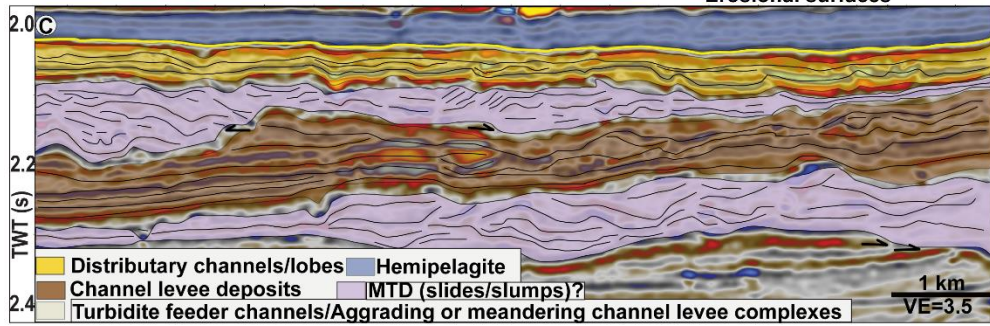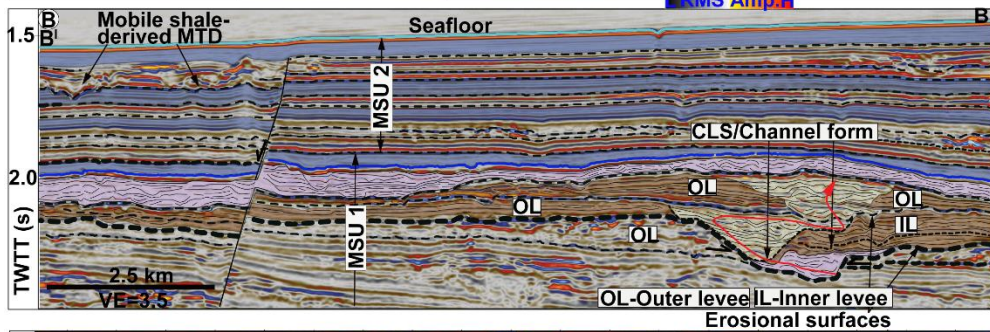
Fig. 2. A: Analysis of the seismic facies. A: Description and interpretation of the facies (modified from Chima *et al.,* 2019). B, C: Association of the facies in and outside the erosional, submarine channels (see Figs. 3C and 5A for their location in panels B and C). See text for a more detailed explanation.
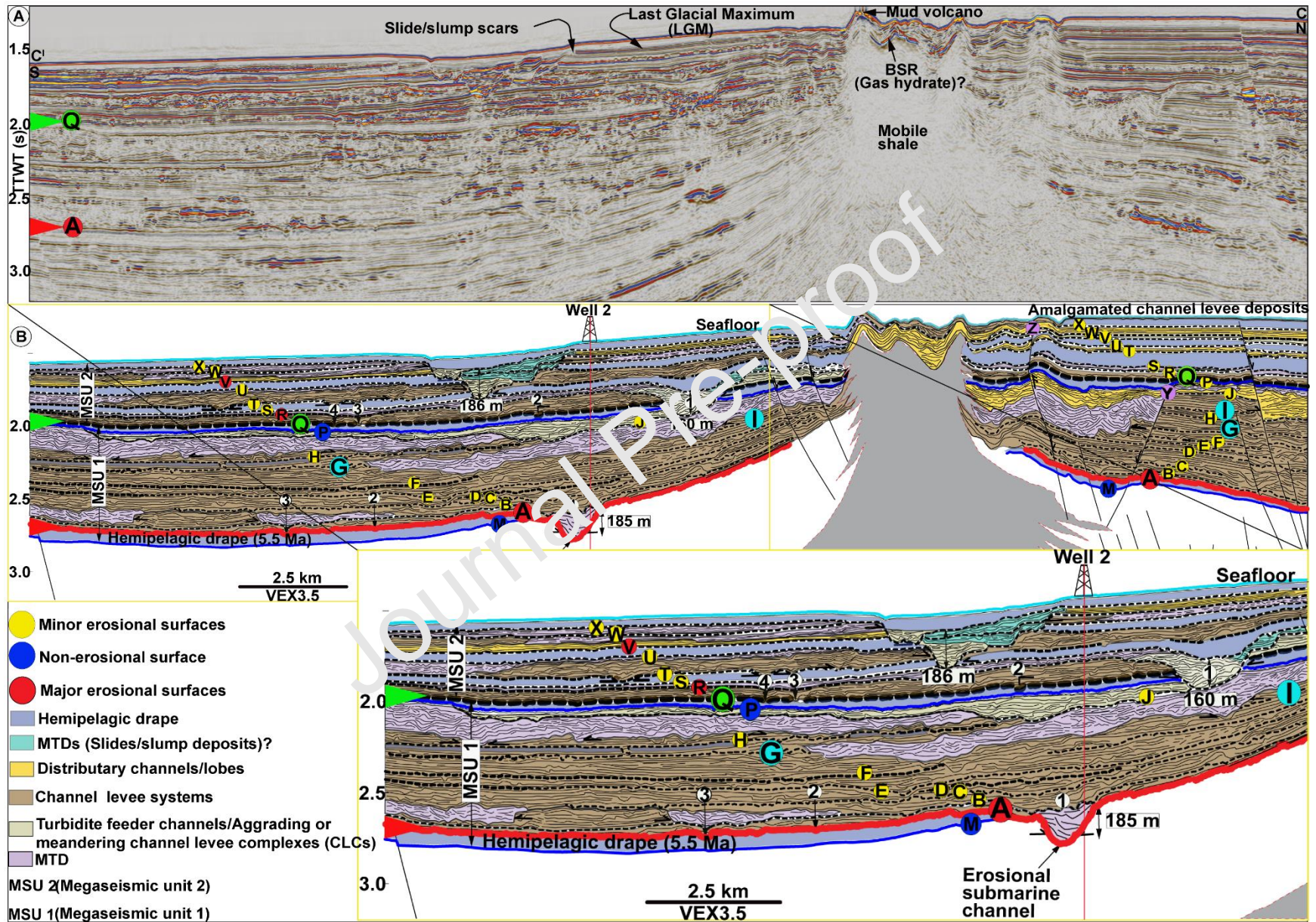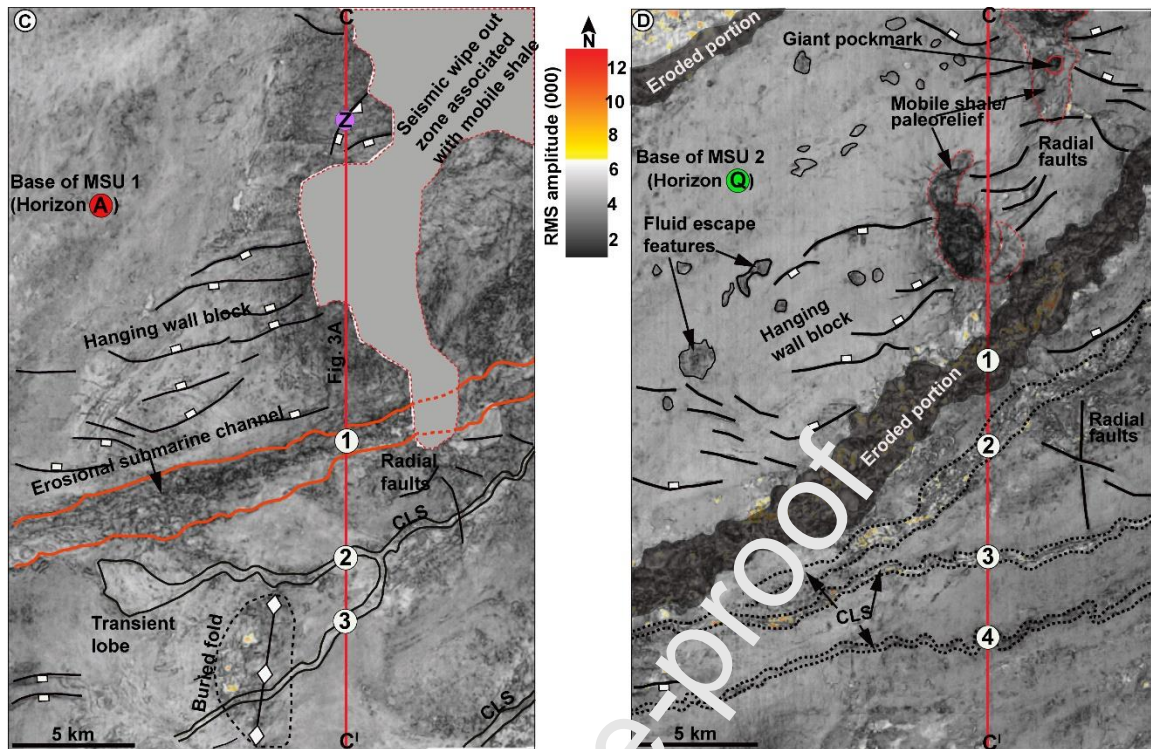
Fig. 3: The Pliocene and Pleistocene stratigraphic architecture of the western Niger Delta intraslope basins. A, B: Uninterpreted north-south seismic line and line drawing (CC[I]), showing the depositional geometries of the MSU 1 and 2 (modified after Chima *et al.,* 2019). Note the lateral thickening of stratigraphy in the MSU 1 away from mobile shale. Yellow arrow points to the base of the hemipelagic drape (horizon M) dated at 5.5 Ma. Letters (M-X) in panel B represent seismic markers. Note the changes in the sedimentary architecture from turbidite-dominated at the lower part of the MSU 1 through a mix of MTDs and turbidites at the upper part of the MSU 1 to hemipelagic drape and turbidites at the transition between the MSU 1 and the MSU 2. Note the lateral truncations of seismic reflections within the MSU 1 compared to the MSU 2. Note also the occurrence of slide/slump scars below the modern seafloor (panel A) and the inverted fault (labelled Z in panel B). C, D: An interpreted RMS amplitude map of the horizons A and P, draped on variance attribute extractions at the lower parts of the MSU 1 and

56

the MSU 2, illustrating the changes in depositional elements. See text for a more detailed explanation.
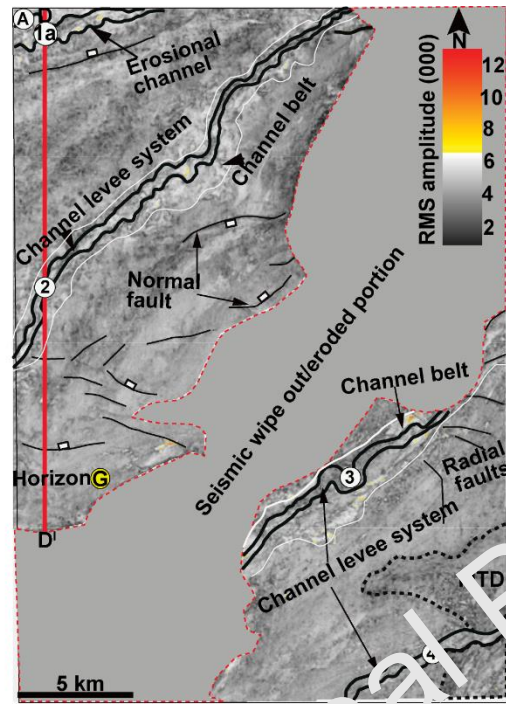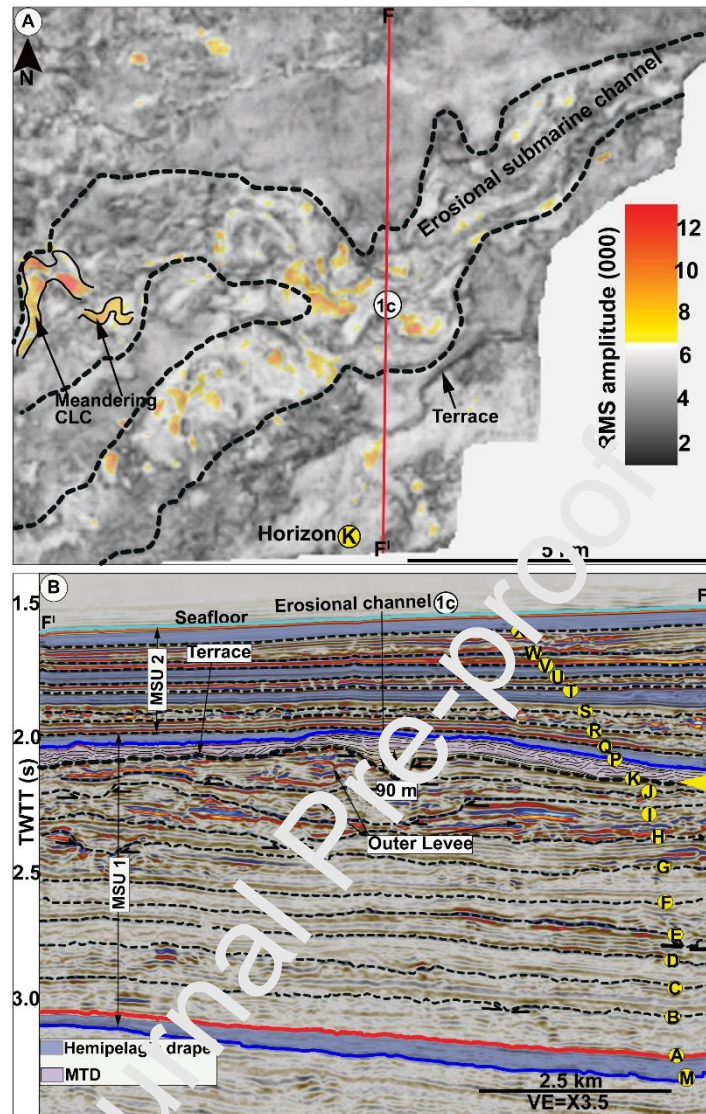
Fig. 4. The sedimentary architecture of the middle part of MSU 1 (horizon G). A: An interpreted RMS amplitude map of horizon G draped on a variance attribute map in the middle part of MSU 1 revealed the presence of sinuous channel levee systems labelled 1a, 2 in the NW, and 3, 4 in the SE parts of the study area. B. Seismic line (DD^I) through channels 1a and 2 illustrates their seismic architecture (1 km wide, 120 m deep). See Fig. 11A for the location of channel 1a in the northern part of the study area.
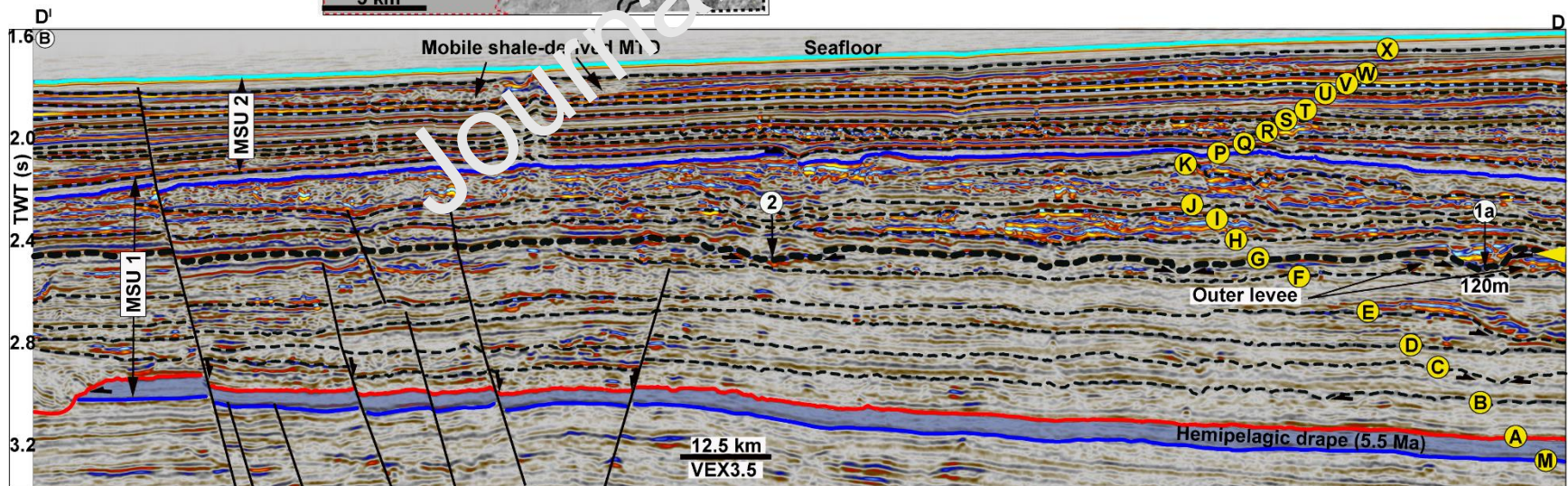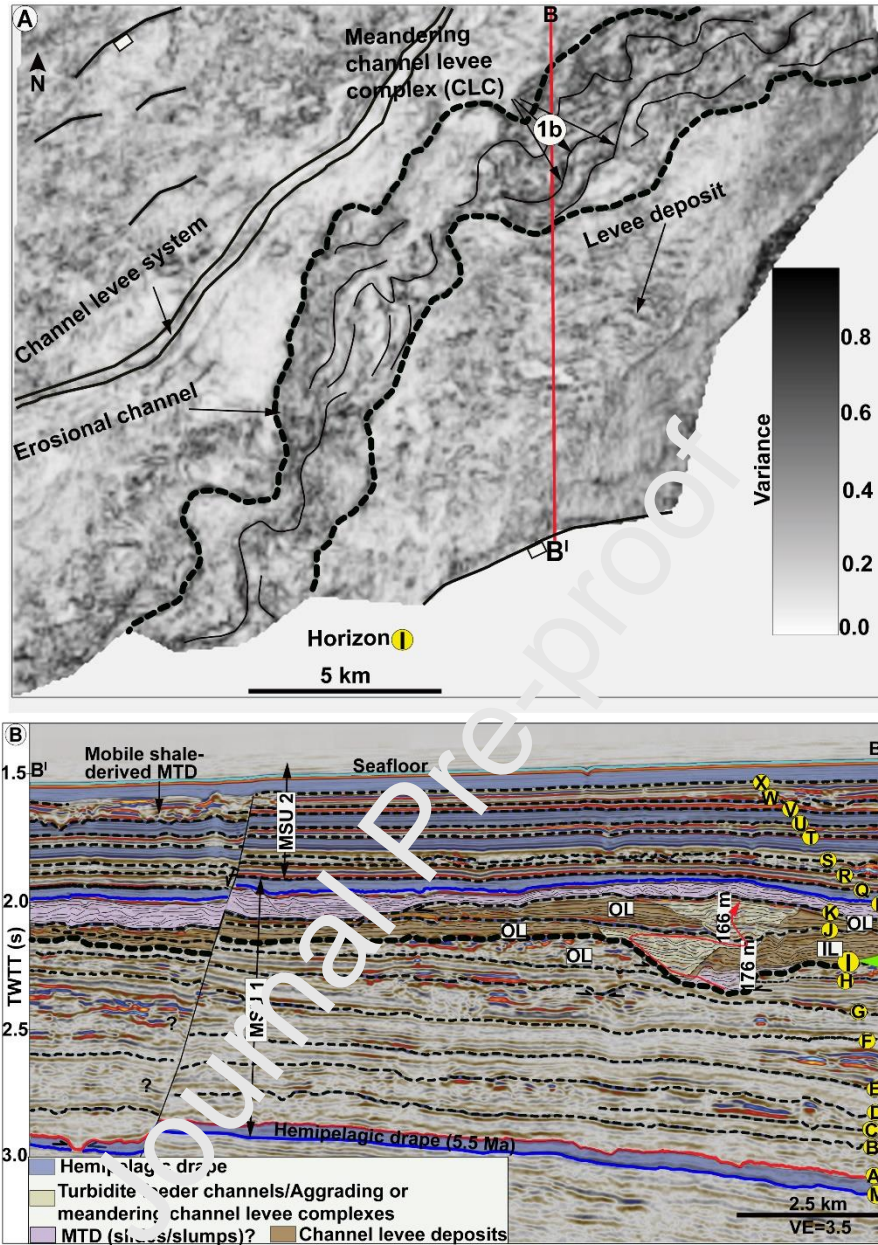
Fig. 5. The sedimentary architecture of the middle part of MSU 1 (horizon I). A: An interpreted variance attribute extraction on horizon I showing the presence of a 2.5 km wide sinuous, erosional channel, characterizsed by meandering CLCs and levee deposits (see yellow arrow in panel B for stratigraphic level). B: Seismic line (EE^I) illustrates the complex cut and fill architecture (176 m deep) of the channel with lateral and vertical aggradational patterns. See Fig. 11A for the location of channel 1b in the northern part of the study area.
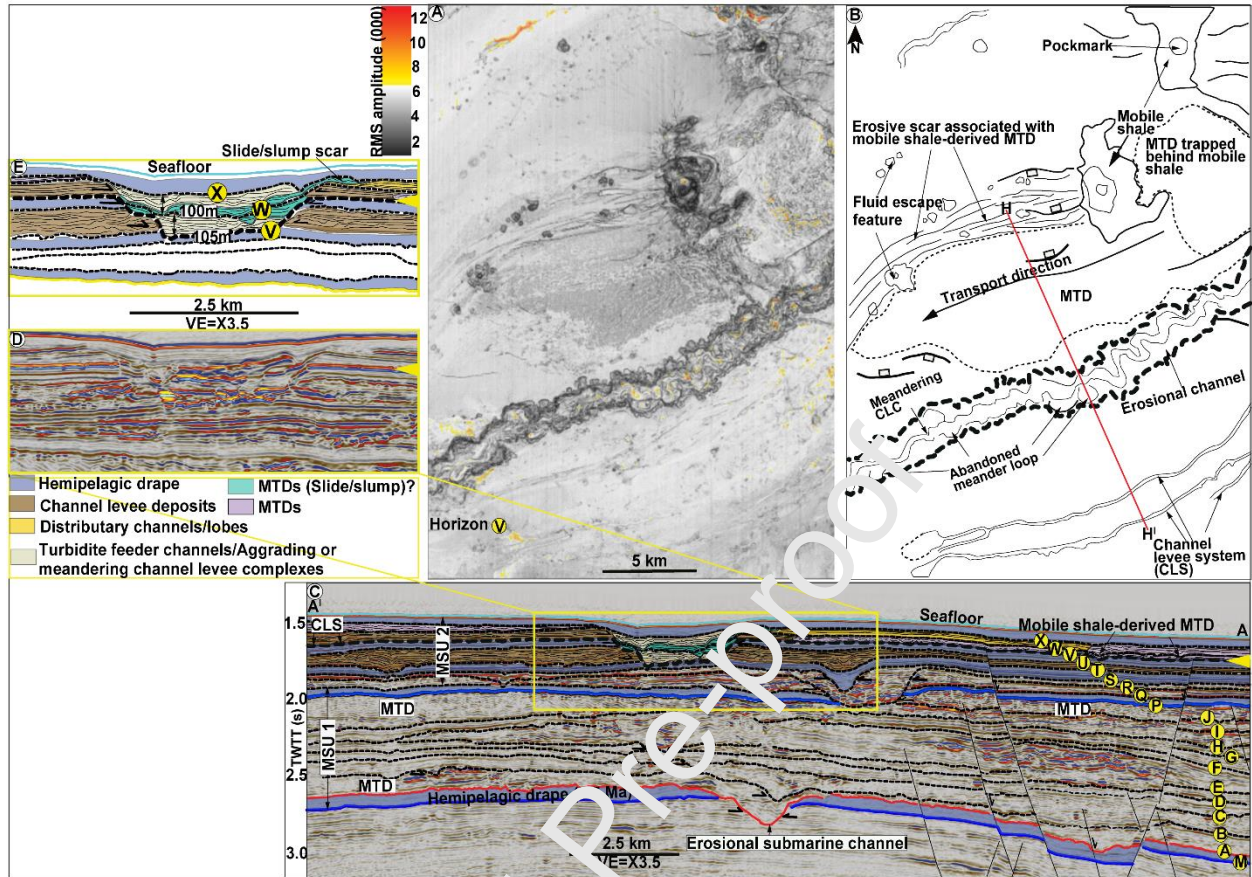
59

Fig. 6. The sedimentary architecture of the upper part of the MSU 1. A: An interpreted RMS amplitude map of horizon K, draped on a variance attribute map, shows the presence of a 1.8 km-wide bifurcating erosional channel, characterised by moderate RMS amplitude and terraces on its outer bend (see yellow arrow in panel B for the stratigraphic level). B: An interpreted north-south seismic line (FF^I), shows the incisional character of the channel (90 m deep), infilled with partially confined, turbidite feeder channels/aggrading or meandering complexes that are truncated by the overlying MTDs (slides/slumps). See Fig. 11A for the location of erosional channel 1c in the northern part of the study area.

60
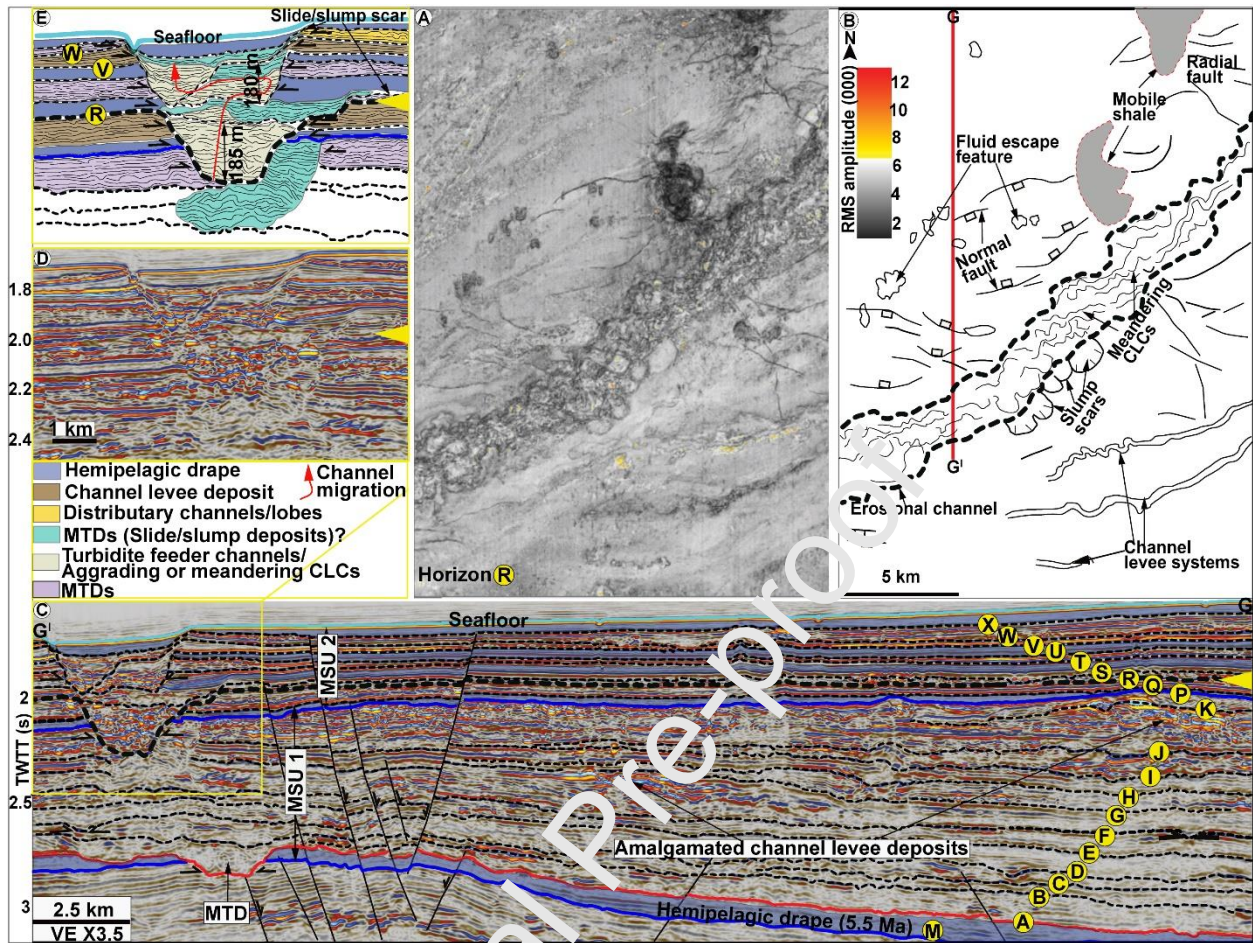
Fig. 7. The sedimentary architecture of the middle part of MSU 2. A, B: An uninterpreted and interpreted RMS amplitude map of the horizon R draped on a variance attribute extraction shows the presence of a 2.5 km-wide channel, characterised by moderate RMS amplitudes and turbidite feeder channels/aggrading or meandering channel levee complexes within the channel axis (see yellow arrow in panel C for the stratigraphic level). C: An interpreted north-south seismic line (GG^I) illustrates the complex cut and fill architecture of the 185 m-deep channel with overall vertical aggradational patterns (panels D, E). Note the upward decrease in the thickness of MTDs (slide/slumps?) and external levee deposits. See text for a more detailed explanation.
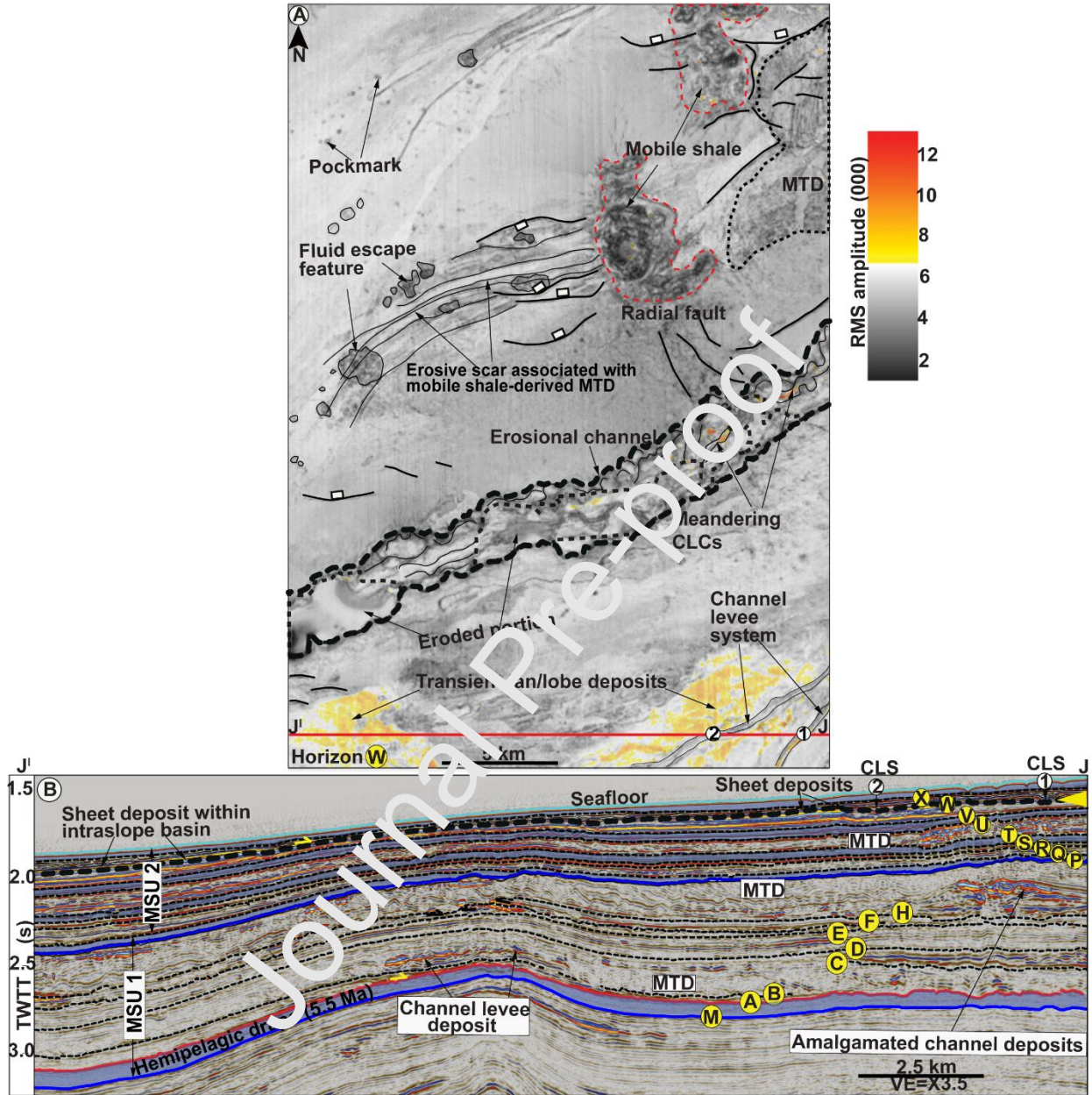
61

Fig. 8. The sedimentary architecture of the upper part of MSU 2. A: An uninterpreted RMS amplitude map of horizon V draped on variance attribute map and B: an interpretation of panel A, shows the presence of a 2.1 km-wide, sinuous erosional submarine channel, characterised by moderate amplitude and turbidite feeder channels/meandering CLCs (see yellow arrow in panel C for the stratigraphic level). Note the upward decrease in the thickness of the MTDs (slide/slumps?) and external levee deposits. C: An interpreted NW-SE seismic line (HH^I) shows the complex cut and fill architecture of the channel (panels D, E). Note the upward decrease in the thickness of the MTDs (slide/slumps?) and external levee deposits. A, B, C (after Chima *et al.*, 2019).

Fig. 9. Sedimentary architecture of the upper part of MSU 2. A: An interpreted RMS amplitude map of horizon W draped on a variance attribute map shows the presence of MTDs trapped behind mobile shale in the north, a 2.5 km wide erosional channel in the central part of the study area and transient fan/lobes, marked by high RMS amplitudes in the south. B: An interpreted E-

W seismic line (JJ^I) illustrates the high reflectivity and onlapping geometry of the transient fans/lobes. Note the presence of mobile shales, mud volcanoes and pockmarks in panel A.
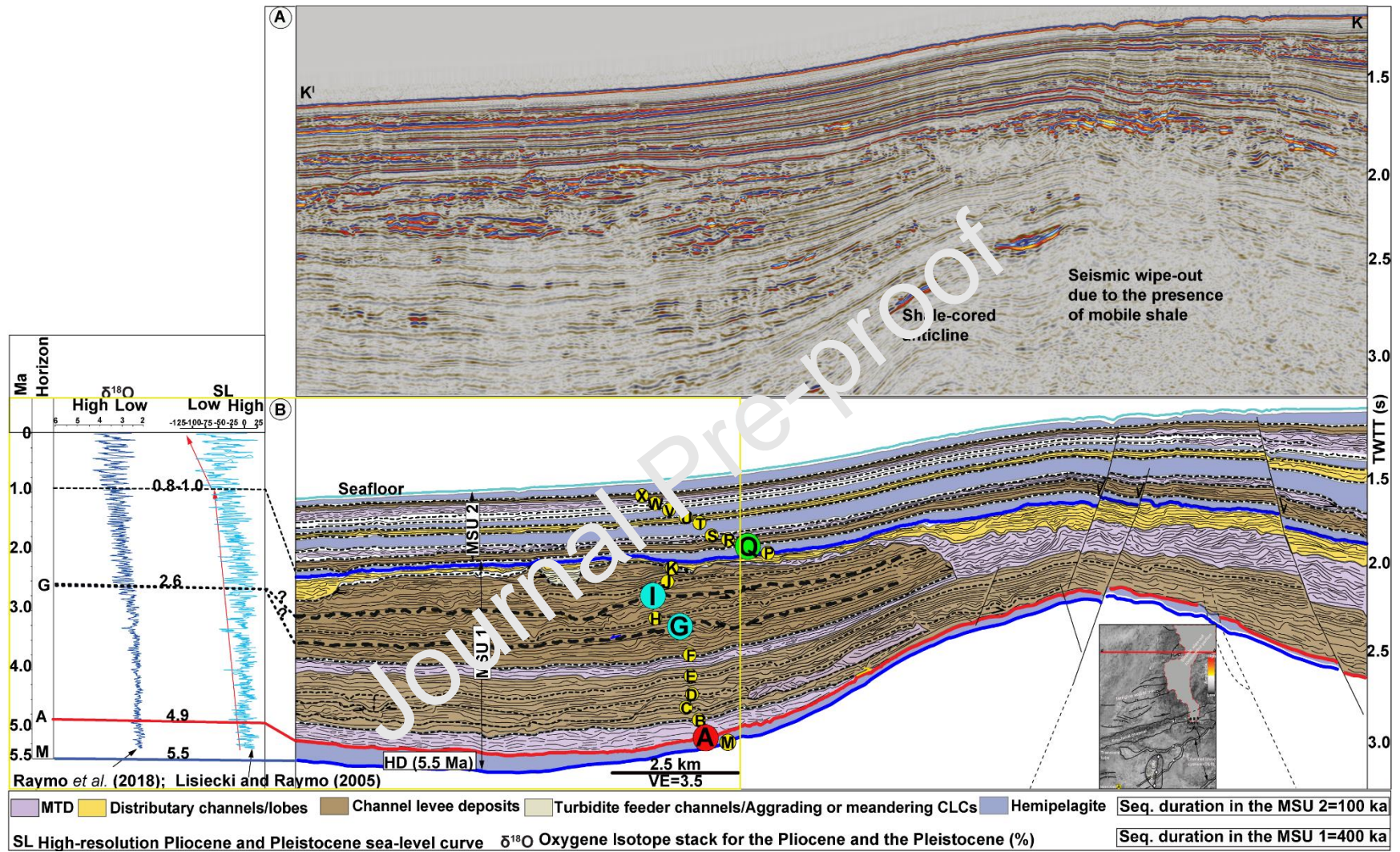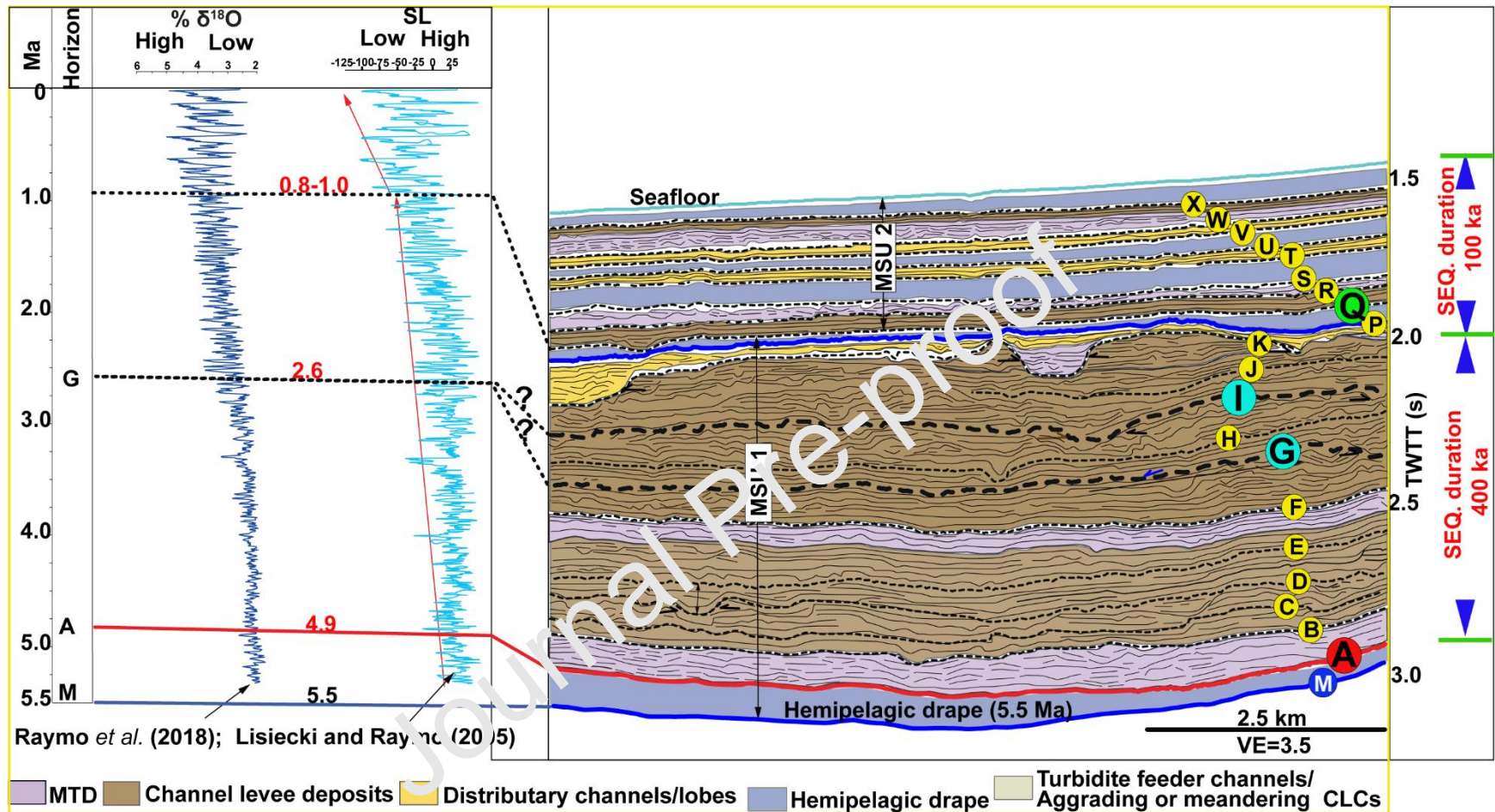
Fig. 10: Sequence stratigraphy. A: An uninterpreted and B: an interpreted E-W seismic and line drawing (KK^I) shows the Pliocene and Pleistocene stratigraphic arichtecture of the western Niger Delta intraslope basins (see detailed view in panel C below). Note the tentative correlation between seismic markers at (the M/A, G/I and K/P) transitions with the sea-level and ^{18}O isotope curves. Note also the lateral variation in the stratigraphic thickness of MSU 2 compared to MSU 1. See text for a more detailed explanation.
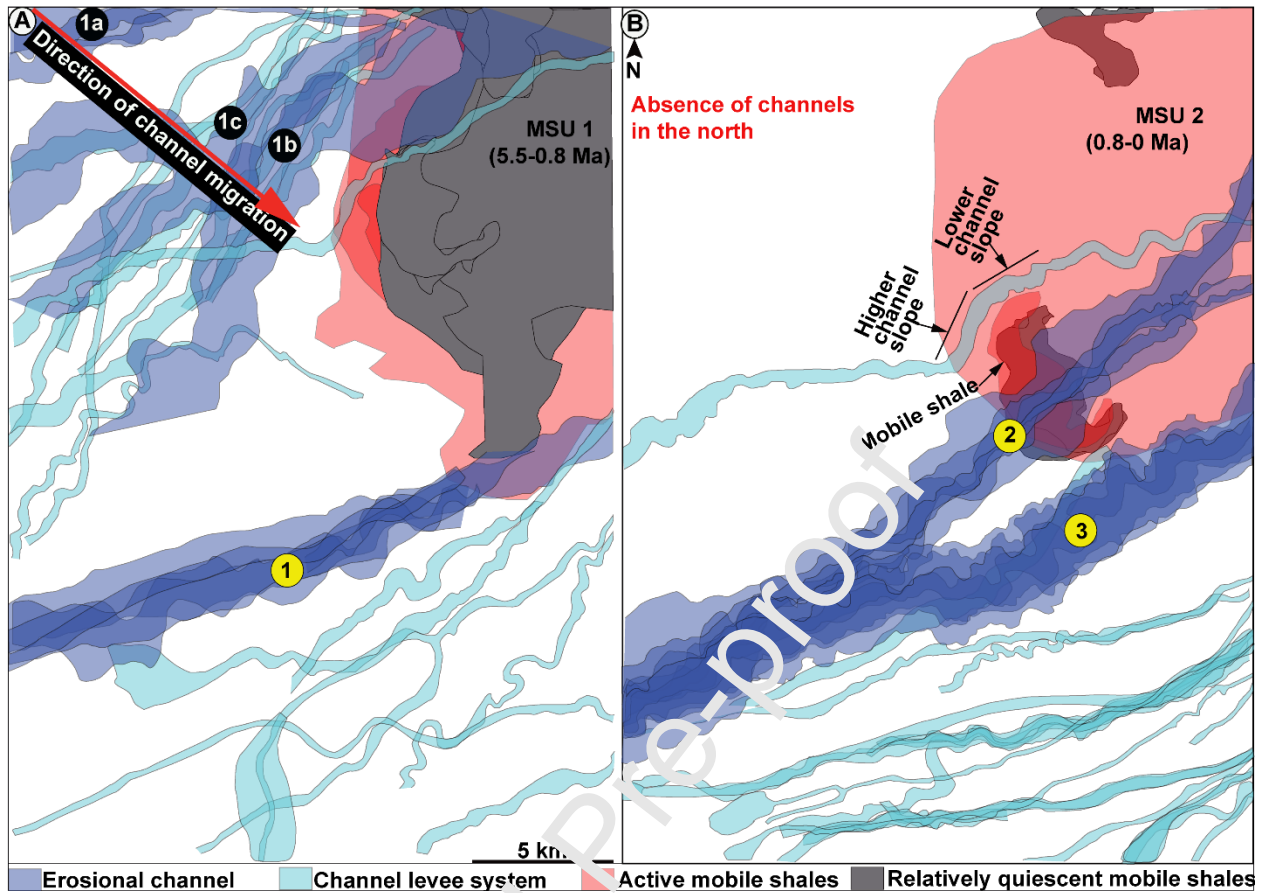
66

Fig. 11. Shale tectonics vs submarine channel morphology and distribution on the western Niger Delta intraslope basins over the last 5.5 Ma. A: Migration of erosional channels from the NW to SE in (stages 1a-c in Figs. 4-6). B: Absence of erosional channels in the northern part of the study area and an increase in the slope of channel levee system (CLS) downdip of mobile shale. Note the space-time variation in the orientation of erosional channels in panels A and B (labelled 1, 2 and 3). A, B (modified after Chima *et al.*, 2019). See text for a more detailed explanation.
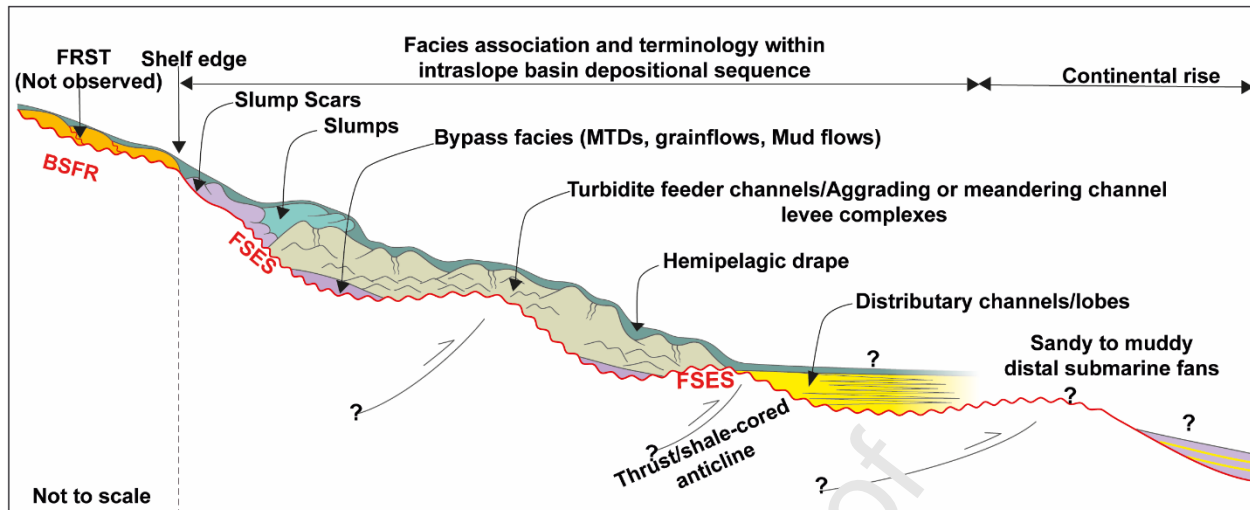
Fig. 12. Schematic illustration of the facies association and terminology used in the western Niger Delta slope depositional model. The falling stage erosional surface (FSES) (this study) is equivalent to the basal surface of forced regression (BSFR) defined on the shelf edge (Posamentier and Kolla, 2003; Catuneanu, 2020) and corresponds to the erosional surfaces observed in MSU 1 and 2 (Figs. 3-10). The FSES is generally overlain by the basal MTDs/bypass facies (where preserved) (e.g. Fig. 5B). The turbidite feeder channels/aggrading or meandering channel levee complexes are the most abundant seismic facies defined between two FSESs and generally overlie the basal MTDs/bypass facies (where preserved; e.g. Fig. 5B) or directly overlie the FSESs (e.g. Figs. 3B; 7C-E, 8C-E). The turbidite feeder channels/aggrading or meandering channel levee complexes are generally overlain/truncated by MTDs (slides/slump?) deposits (e.g. Figs. 3B; 7C-E, 8C-E). The entire system is generally covered by hemipelagic drape/muddy turbidites where preserved (e.g. Figs. 3B; 7C-E, 8C-E). See section 5.3 for a more detailed explanation.
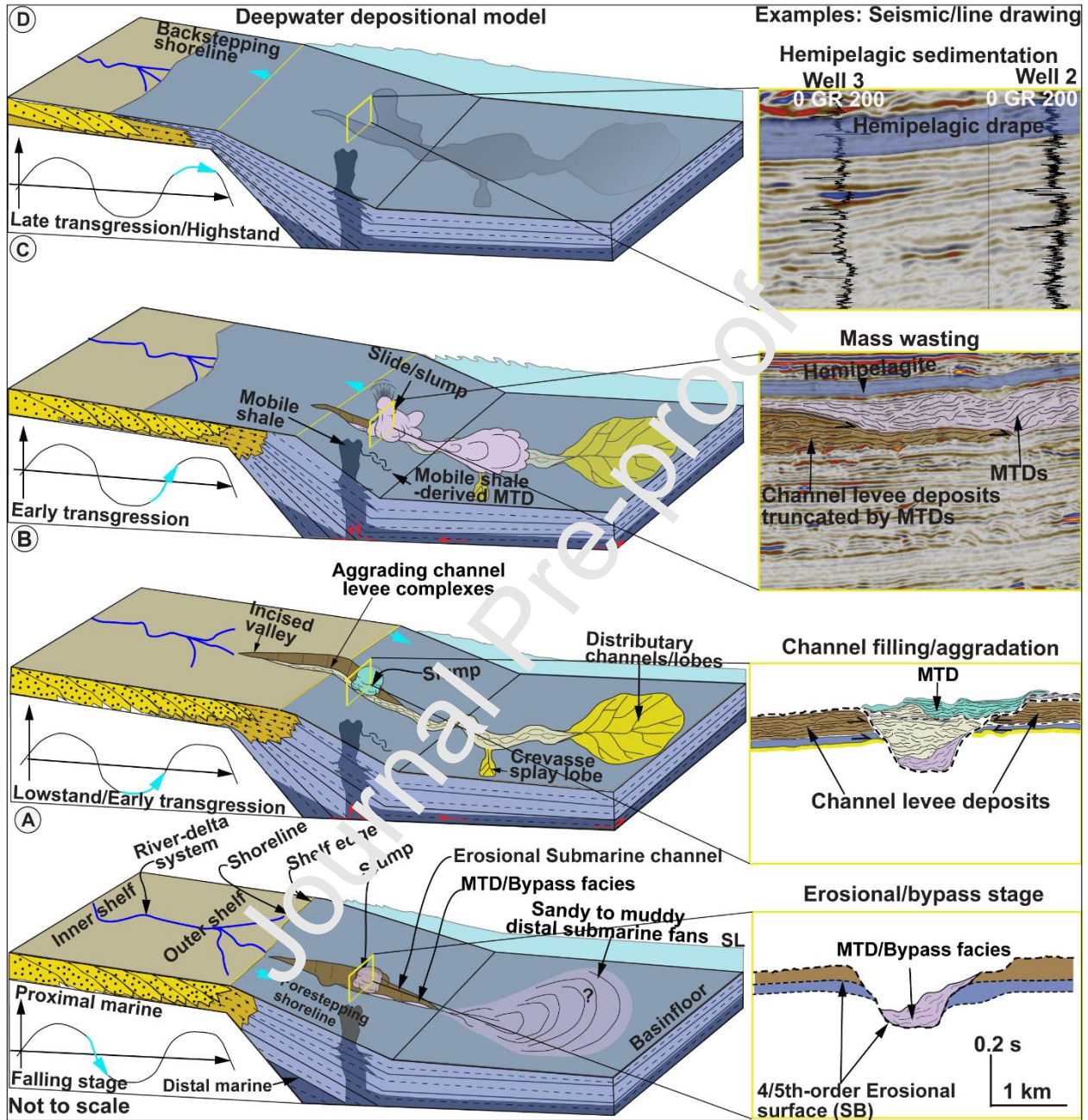
Fig. 13. Proposed depositional model illustrating the long-term Pliocene and Pleistocene stratigraphic evolution of the western Niger Delta intraslope basins with respect to fourth/fifth-order relative sea-level changes, locally influenced by shale tectonics. A: The falling stage marks the developemnt of erosional submarine channels/falling stage erosional surfaces (FSESs) and

MTDs (bypass facies). B: The lowstand/early transgression marks the infilling/aggradation of erosional submarine channels C: Early/late trangression marks the onset of draping of submarine channels and the development of mass wasting that partially truncate the underlying lowstand deposits. D: The late trangressive/highstand stage marks the hemipelagic draping of erosional submarine channel complexes and the end of deepwater sedimention. Stages A-E are summarised in Fig. 13E.
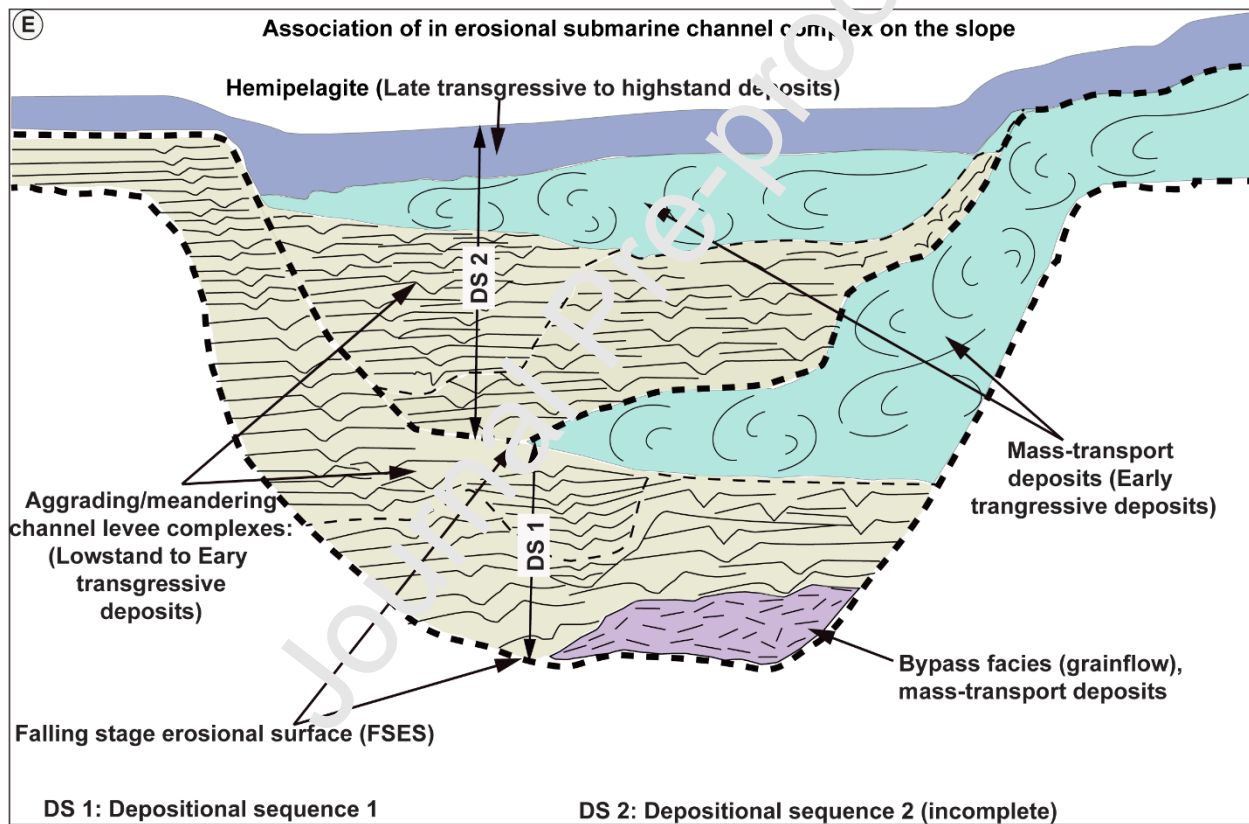

Fig. 13 E: Schematic illustration of facies association and systems tracts in the erosional submarine channel complex on the slope.

Highlights

- Seq. cycles linked to the Milankovitch cycles are recorded regionally on the Niger Delta slope

- The early Pliocene-mid Pleist. (5.5-0.8 Ma) is dominated by 400 ka eccentricity sequences

- The mid Pleist.-present (0.8-0 Ma) is dominated by 100 ka eccentricity sequences

- Increase in sedimentation rates at the MPT facilitated the preservation of the 100 ka sequences.

- Glacio-eustatic and shale tectonic forcings controlled the Pliocene and Pleistocene stratigraphy